AdaptiveMedStego: A High-Capacity Reversible Medical Image Steganography Method Based on Adaptive Multi-Level Wavelet Transform

Ya Qiu, Xinchao Wang, Chenrui Fu, Xingyu Kang, Yuhao Cui

***Abstract*-This paper presents AdaptiveMedStego, a medical-image steganography method that integrates multi-level wavelet transform, singular-value decomposition (SVD), and QR decomposition to embed data securely while preserving image quality. The proposed algorithm automatically detects diagnostically significant regions and applies region-dependent embedding strategies. Experiments on CT, MRI, X-ray, and ultrasound images show that AdaptiveMedStego achieves higher embedding capacity and superior image quality than state-of-the-art techniques. By adapting the embedding strength to regional importance, it maintains diagnostic clarity even at high payloads. Although the method demands more computational power than simpler approaches, it performs consistently well across diverse image types. AdaptiveMedStego therefore advances data hiding in medical images by balancing capacity, quality, and security, and it provides a foundation for future research on adaptive steganography in healthcare.**

***Index Terms*-Medical image steganography, wavelet transform, adaptive embedding, image quality preservation, data security, healthcare informatics, diagnostic accuracy, computational efficiency**

I. Introduction

Telemedicine has experienced significant growth over the past decade, establishing itself as an essential component of modern healthcare. By leveraging information and communication technologies, healthcare professionals can deliver diagnostic, treatment, and follow-up services across geographical barriers. Consequently, telemedicine has improved access to medical resources for remote populations and has proved invaluable during global health crises such as the COVID-19 pandemic [1].

However, this expansion has brought data security and patient privacy to the forefront [2]. Medical data—especially electronic health records (EHRs) that contain sensitive personal information—require robust protection during transmission, storage, and processing. Unauthorized access or data tampering can lead to privacy violations and potentially incorrect medical decisions, thereby endangering patient safety. Regulatory frameworks such as the General Data Protection Regulation (GDPR) in Europe and the Health Insurance Portability and Accountability Act (HIPAA) in the United States impose strict requirements for handling medical data [3], underscoring the critical need for strong security measures in telemedicine. Researchers are therefore developing innovative solutions, including advanced encryption, secure communication protocols, blockchain applications, and AI-based anomaly-detection systems [4]. Achieving an optimal balance among security, usability, and efficiency remains a major challenge.

Medical image steganography is a pivotal technology for healthcare data security, particularly in telemedicine and digital health records [5]. It embeds sensitive patient information directly into medical images—such as X-rays, CT scans, or MRIs—while preserving their visual quality and diagnostic value [6]. By concealing information within the images themselves, sensitive data can be transmitted and stored inconspicuously, protecting it from unauthorized access [7]. This capability is especially valuable in telemedicine, where medical images and associated patient information routinely traverse potentially vulnerable networks. Moreover, medical image steganography helps healthcare providers comply with HIPAA and GDPR by securely linking patient data with corresponding images [8], thereby streamlining workflows, reducing the risk of mismatches, and ultimately enhancing patient care and safety.

Recent advances have focused on methods that effectively hide data while maintaining diagnostic quality [9]. These approaches exploit the specific characteristics of different imaging modalities to maximize embedding capacity and minimize image distortion [10]. As healthcare systems continue to digitize and the volume of medical imaging grows, steganography plays a vital role in safeguarding patient information's confidentiality, integrity, and availability. It has thus become an integral component of

Manuscript received March 4, 2025; revised July 21, 2025.

This work was financially supported by Henan Province Science and Technology Research and Development Joint Fund Program (No. 235101610024), Nanyang Science and Technology Key Project (No. 23KJGG008), and Innovation and Entrepreneurship Training Program for College Students of Henan Province (No. 202411653026).

Ya Qiu is a Lecturer in School of Computer and Software, Nanyang Institute of Technology, Nanyang 473004, China (corresponding author to provide e-mail: 3162060@nyist.edu.cn).

Xinchao Wang is a Lecturer in College of Information Engineering, Nanyang Vocational College of Agriculture, Nanyang 473000, China (e-mail: wxc739@163.com).

Chenrui Fu is an undergraduate student in School of Computer and Software, Nanyang Institute of Technology, Nanyang 473004, China (email: 2906903162@qq.com).

Xingyu Kang is an undergraduate student in School of Computer and Software, Nanyang Institute of Technology, Nanyang 473004, China (email: 2215925572@nyist.edu.cn).

Yuhao Cui is an undergraduate student in School of Computer and Software, Nanyang Institute of Technology, Nanyang 473004, China (email: 2215925567@nyist.edu.cn).

contemporary healthcare security infrastructure.

Despite substantial progress, current medical image steganography techniques face several limitations that hinder widespread clinical adoption. Chief among these are the challenges of balancing embedding capacity, image quality, security, and computational efficiency. Embedding sufficient data without introducing distortions that compromise diagnostic accuracy is difficult—subtle alterations can lead to misdiagnosis. Security is another concern: many methods remain vulnerable to steganalysis [11]. Additionally, limited resilience to common image processing operations (e.g., compression, scaling) restricts real-world applicability [12]. High computational demands pose further obstacles, particularly for real-time telemedicine applications [13]. Many techniques also overlook modality-specific characteristics, applying generic methods unsuitable for particular image types such as CT scans, MRIs, or ultrasounds. Finally, a lack of standardization complicates integration with existing healthcare information systems, impeding interoperability [14].

This research therefore proposes an advanced medical image steganography method designed to overcome these limitations while meeting modern healthcare demands. The algorithm intelligently selects non-diagnostic regions for embedding, thereby minimizing clinical impact; preserves hidden-data integrity against common image operations; incorporates an efficient encryption scheme to resist steganalysis; and adapts flexibly to various imaging modalities.

The main contributions of this work are as follows:

(1) We introduce a novel adaptive multi-level wavelet transform and threshold selection strategy that dynamically balances embedding capacity with image quality preservation.

(2) We propose a collaborative security mechanism that combines SVD and QR decomposition to improve the robustness and security of the embedded data against steganalysis attacks.

(3) We develop a region-adaptive embedding strategy that intelligently identifies critical diagnostic areas, applying conservative embedding to preserve clinical value while maximizing capacity in non-critical regions.

(4) We implement and validate a fully reversible data hiding mechanism, ensuring that the original medical image can be perfectly reconstructed, which is critical for clinical and legal purposes.

II. Related Works

A. Medical Image Steganography Techniques

Medical image steganography has seen considerable advancements in recent years, with researchers developing innovative methods to enhance embedding capacity, preserve image quality, and bolster security. Parah et al. [6] introduced a high-capacity reversible data hiding technique for medical images using interpolation and histogram shifting. Their approach significantly increased embedding capacity while preserving diagnostic quality across diverse imaging modalities, such as MRI and CT scans.

To address challenges in preserving image quality, Al-Haj and Hussein [8] proposed a hybrid method combining Discrete Wavelet Transform (DWT) and Singular Value Decomposition (SVD). This approach demonstrated enhanced robustness against JPEG compression and noise addition, facilitating secure medical image transmission. In the realm of adaptive steganography, Usman et al. [15] created a technique that intelligently selects embedding regions based on specific medical image characteristics, prioritizing non-diagnostic areas in X-rays to minimize impact on critical diagnostic information. Seeking improved security, El-Latif et al. [16] designed an encryption-then-embedding scheme. Their method utilized a chaotic system for initial data encryption, followed by an enhanced Least Significant Bit (LSB) substitution technique, which significantly strengthened resistance against statistical analysis attacks. Liu et al. [17] advanced reversible data hiding through prediction-error expansion, enabling complete recovery of original medical images alongside error-free data extraction-a capability essential for forensic and clinical research applications where image integrity is paramount. Recent innovations include the integration of artificial intelligence (AI) into medical image steganography. Jain et al. [18], for example, employed deep learning, specifically a Convolutional Neural Network (CNN)-based approach, to automatically determine optimal embedding locations and strengths. Their method showed promising results in enhancing both the efficiency and imperceptibility of embedded data.

B. Applications of Wavelet Transform in Image Processing

Wavelet transformation has emerged as an essential tool in image processing applications, especially in medical imaging, offering multi-resolution analysis and efficient feature representation. For medical image compression, Uthayakumar et al. [19] developed an innovative approach combining wavelet transform with entropy encoding. This method achieved high compression ratios while retaining critical diagnostic information in MRI and CT images. The multi-resolution capabilities of wavelets enabled adaptive compression, allowing regions of interest to be preserved at higher quality than background areas.

For medical image denoising, Rajini and Bhavani [20] introduced a wavelet-based technique that effectively removes Gaussian and speckle noise from ultrasound images. By separating signal from noise across different scales, their method preserves edge information while improving overall image quality. In the domain of multi-modal image fusion, Singh and Khare [21] devised a wavelet-based algorithm to combine information from Positron Emission Tomography (PET) and MRI scans. By decomposing images into various

frequency bands, their method facilitates a more effective integration of complementary data from these distinct imaging modalities. Wavelets have also proven valuable for feature extraction in medical image analysis. Nithya and Santhi [22] utilized wavelet-based texture features to classify brain tumors in MRI images. The multi-scale characteristics of wavelets enabled the extraction of both global and local texture features, thereby enhancing tumor detection and classification accuracy. To address low-contrast medical images, Gan et al. [23] introduced a contrast enhancement technique using wavelet decomposition. Their approach involves applying adaptive histogram equalization in the wavelet domain to improve the visibility of subtle structures in X-rays and mammograms. In medical image segmentation, Shih and Tseng [24] developed a wavelet-based edge detection algorithm. This algorithm captures sharp transitions across multiple scales, providing more accurate and robust edge detection in complex medical images compared to conventional gradient-based methods.

These applications collectively underscore the versatility and effectiveness of wavelet transformation in addressing diverse challenges within medical image processing. The inherent ability of wavelets to simultaneously provide spatial and frequency information makes them exceptionally well-suited for tasks demanding both the preservation of critical image features and efficient data manipulation.

III. AdaptiveMedStego Method

A. System Architecture Overview

AdaptiveMedStego presents a comprehensive framework that addresses the complex challenge of embedding sensitive patient data in medical images while preserving diagnostic quality and ensuring security. This innovative approach combines several advanced techniques to create a robust and adaptable steganographic system.

The core of AdaptiveMedStego is a multi-level wavelet transform engine that serves as the foundation for our adaptive embedding strategy. This component breaks down medical images into multiple sub-bands, enabling flexible data embedding across various scales and frequencies. Complementing this is an adaptive threshold selection unit that dynamically assesses each sub-band's characteristics to determine optimal embedding parameters, balancing data capacity with visual quality. A key feature is the system's intelligent region handling through a sophisticated ROI analyzer, which uses advanced image processing and machine learning to identify critical diagnostic areas. This guides the adaptive embedding engine to apply different strategies to diagnostically important regions versus less sensitive areas. Security is enhanced through a dual decomposition approach using SVD and QR decomposition, which works on selected wavelet coefficients to add protection to the steganographic process. The system includes a reversible data hiding unit ensuring complete recovery of original images after data extraction-essential for maintaining medical record integrity. To address various medical imaging types, we've incorporated a cross-modal adaptation layer that adjusts embedding parameters based on specific characteristics of different modalities like X-rays, MRIs, and CT scans. Finally, anticipating AI's growing role in medical diagnosis, we've integrated an AI-friendly feature preservation mechanism that ensures the steganographic process preserves image features critical for automated analysis and computer-aided diagnosis.

The entire system is wrapped in a comprehensive security and encryption module that handles both data encryption before embedding and cryptographic key management. This final security layer ensures that even if hidden data is detected, its contents remain protected. AdaptiveMedStego functions as an integrated pipeline where components sequentially process and transfer data, enabling efficient parallel processing where feasible. The architecture features strategic feedback loops, particularly between the adaptive threshold selection unit and embedding engine, allowing real-time optimization based on each image's unique characteristics and the embedded data, as illustrated in Fig. 1.

B. Multi-level Wavelet Transform and Adaptive Threshold Selection

Optimal Decomposition Level Selection Strategy

Multi-level wavelet transforms forms the foundation of AdaptiveMedStego, offering a multi-resolution analysis framework for medical image steganography. Selecting the optimal decomposition level is essential to balance embedding capacity, image quality, and computational efficiency. Our approach to determining this optimal level integrates several key factors into a comprehensive strategy.

The theoretical maximum decomposition level L_{max} for an image of size $M \times N$ is given by $L_{max} = floor\left(log2(min(M,N))\right)$. However, this upper bound does not necessarily yield the most suitable decomposition for steganographic purposes. To refine this selection, we analyze the energy distribution across decomposition levels. The energy ratio E_j at level j is defined as.

$$E_j = \left(LL_j^2 + LH_j^2 + HL_j^2 + HH_j^2\right)/\left(LL_{j-1}^2\right) \quad (1)$$

where LL, LH, HL, and HH represent the low and high frequency sub-bands respectively. This energy analysis provides insights into the information content at each level, guiding our decision on the appropriate depth of decomposition.

Furthermore, we incorporate a structural similarity assessment to evaluate the impact of each decomposition level on the image's diagnostic value. The Structural Similarity Index (SSIM) between the original image x and the reconstructed image y at each level is computed as

$$SSIM(x,y) = (2\mu_x\mu_y + C_1)(2\sigma_x y + C_2)/\left((\mu_x^2 + \mu_y^2 + C_1)(\sigma_x^2 + \sigma_y^2 + C_2)\right) \quad (2)$$

where μ and σ denote mean and standard deviation, respectively, and C_1 and C_2 are constants to stabilize the division.

Our adaptive algorithm iteratively evaluates these metrics, beginning with the maximum level L_{max} and decrementing until either the energy ratio falls below a threshold T_E or the SSIM drops below a threshold T_{SSIM}. The optimal level L_{opt} is then determined as the last level that satisfies both criteria. To allow for fine-tuning between embedding capacity and image quality, we introduce an adaptive parameter α, computing the final decomposition level as

$$L_{final} = round\big(\alpha * L_{opt} + (1-\alpha) * L_{max}\big) \quad (3)$$

where $\alpha \in [0,1]$ can be adjusted based on specific application requirements.

This strategy ensures that the selection of decomposition levels not only considers the intrinsic characteristics of the image but also adapts to various medical imaging modalities and steganographic needs. By dynamically adjusting the decomposition level, we maximize the potential for data embedding while maintaining diagnostic quality. Moreover, to address computational efficiency concerns, particularly in time-sensitive medical applications, we incorporate a time threshold T_{time}. If the computation time exceeds T_{time}, we limit L_{final} to the current computed level, ensuring the process remains within acceptable time constraints.

Adaptive Threshold Algorithm Design

Building on the decomposition level selection strategy, our adaptive threshold algorithm determines optimal embedding intensity across wavelet subbands. This approach maximizes data capacity while preserving both the visual quality and diagnostic value of medical images.

The adaptive threshold algorithm operates on each subband resulting from the multi-level wavelet decomposition. For a given subband S_j at decomposition level j, we compute the local variance $\sigma_j^2(x,y)$ in a neighborhood $N(x,y)$ around each coefficient:

$$\sigma_j^2(x,y) = (1/|N(x,y)|) \sum(u,v) \in N(x,y) \left(S_j(u,v) - \mu_j(x,y)\right)^2 \quad (4)$$

where $\mu_j(x,y)$ is the local mean. This local variance serves as an indicator of the textural complexity and edge information in different regions of the subband. We then define an adaptive threshold $T_j(x,y)$ for each coefficient:

$$T_j(x,y) = k * \sigma_j(x,y) * \left(1 - e^{(-\lambda * |S_j(x,y)|)}\right) \quad (5)$$

where k is a scaling factor, λ is a sensitivity parameter, and $|S_j(x,y)|$ is the magnitude of the wavelet coefficient. This formulation allows for higher thresholds in areas of high variance (typically corresponding to edges or textured regions) and lower thresholds in smooth areas.

To account for the varying importance of different subbands, we introduce a level-dependent weighting factor w_j:

$$w_j = 2^{(-j/2)} \quad (6)$$

This factor assigns higher weights to lower frequency subbands, which typically contain more visually significant information. The final adaptive threshold $T_{final_j}(x,y)$ is then computed as:

$$T_{final_j}(x,y) = w_j * T_j(x,y) \quad (7)$$

This threshold is used to determine the number of least significant bits (LSBs) that can be modified in each wavelet coefficient for data embedding. Coefficients with values exceeding their corresponding threshold are candidates for embedding, with the number of modifiable LSBs proportional to the excess over the threshold.

To ensure compatibility with the optimal decomposition level selection, we incorporate the energy ratio E_j and SSIM metrics from the previous stage. The adaptive threshold is further adjusted based on these metrics:

$$T_{adjusted_j}(x,y) = T_{final_j}(x,y) * \left(1 + \beta * (1 - SSIM_j)\right) * (1 + \gamma * E_j) \quad (8)$$

where β and γ are weighting factors that control the influence of structural similarity and energy distribution, respectively. This comprehensive adaptive thresholding approach ensures that the data embedding process is finely tuned to the characteristics of each medical image, preserving critical diagnostic features while maximizing steganographic capacity. The algorithm for Multi-level Wavelet Transform and Adaptive Threshold Selection is explained in **Algorithm 1**.

C. Secure Embedding Combining SVD and QR Decomposition

Collaborative Mechanism of SVD and QR Decomposition

The AdaptiveMedStego method innovatively combines SVD and QR decomposition to enhance the security and robustness of data embedding in medical images. This collaborative mechanism operates on the wavelet subbands selected for embedding, providing an additional layer of data protection. For a given wavelet subband W, we first apply SVD:

$$W = USV^T \quad (9)$$

where U and V are orthogonal matrices, and S is a diagonal matrix of singular values. The singular values in S represent the energy distribution of the subband and are less sensitive to small perturbations, making them suitable candidates for data embedding. We then apply QR decomposition to the matrix S:

$$S = QR \quad (10)$$

where Q is an orthogonal matrix and R is an upper triangular matrix. The QR decomposition further disperses the energy and introduces additional degrees of freedom for data hiding.

The data embedding process is then performed on the R matrix. Let R' be the matrix after embedding the secret data. The modified subband W' is reconstructed as:

$$W' = U(QR')V^T \quad (11)$$

This dual decomposition approach provides multiple benefits. It scatters embedded data across different image components, enhancing resilience against attacks. The orthogonal transformations maintain subband energy, preserving overall image quality. Additionally, combining SVD and QR decomposition creates multiple transformation domains, significantly complicating unauthorized access attempts.

The embedding process itself utilizes a modified bit-plane manipulation technique. For each element r_{ij} in R, we determine the number of bits k that can be modified based on the adaptive threshold T_{ij}:

$$k = floor\left(log2\left(|r_{ij}|/T_{ij}\right)\right) \quad (12)$$

The k least significant bits of r_{ij} are then replaced with k bits from the secret data. This adaptive approach ensures that more bits are embedded in coefficients with larger magnitudes, which are typically more robust to modifications.

To further enhance security, we introduce a pseudo-random permutation P to scramble the order of bit embedding:

$$r'_{ij} = Embed\left(r_{ij}, P\left(secret_{data_k}\right)\right) \quad (13)$$

where $Embed()$ is the bit replacement function and $P()$ is the permutation function. This permutation is governed by a secret key, adding an extra layer of security to the embedding process.

The combination of SVD and QR decomposition with adaptive thresholding and permutation-based embedding creates a strong, secure system for protecting sensitive medical image data. This integrated approach enhances both the invisibility of embedded information and substantially increases protection against unauthorized access or manipulation.

Security Enhancement Strategies

Building on the SVD and QR decomposition foundation, we implement several advanced security strategies to strengthen AdaptiveMedStego against potential attacks and unauthorized access.

Firstly, we introduce a dynamic key generation scheme based on image characteristics. Let K be the base key, and $H(W)$ be a hash function of the original wavelet subband W. We compute an image-dependent key K_i as:

$$K_i = K \oplus H(W) \quad (14)$$

where $\oplus$ denotes bitwise XOR operation. This ensures that each image has a unique embedding key, enhancing the system's resistance to replay attacks.

We then employ a block-wise embedding strategy to increase the method's resilience against cropping and localized attacks. The R matrix from QR decomposition is divided into non-overlapping blocks B_m of size $b \times b$. For each block, we compute a block-specific embedding strength α_m:

$$\alpha_m = f(\sigma_m, \mu_m, E_m) \quad (15)$$

where σ_m is the block's standard deviation, μ_m is its mean, and E_m is its edge density. The function f is designed to assign higher embedding strengths to textured or edge-rich areas, which can better mask the embedded data.

To counter statistical attacks, we implement an adaptive dither modulation. For each coefficient r_ij in block B_m, the embedded value r'_{ij} is computed as:

$$r'_{ij} = r_{ij} + \alpha_m * d_{ij} * q \quad (16)$$

where d_{ij} is a dither signal generated from K_i, and q is the quantization step. This modulation introduces controlled distortions that mimic natural image variations, making statistical detection more challenging.

We also incorporate an error correction coding (ECC) scheme to enhance the robustness of embedded data. Using Reed-Solomon codes, we encode the secret data S into a redundant form S_{ecc}:

$$S_{ecc} = RS_{encode}(S, t) \quad (17)$$

where t is the error correction capability. This allows the system to recover from partial data loss or corruption during the extraction process.

To protect against unauthorized extraction attempts, we implement a multi-level authentication protocol. Let A be the authentication data derived from both the image and the secret data:

$$A = g(W, S, K_i) \quad (18)$$

where g is a cryptographic hash function. This authentication data is embedded alongside the secret information, allowing for integrity verification during extraction.

Lastly, we employ a selective bit-plane confusion technique. Based on K_i, we selectively swap certain bit-planes of the embedded data within each block:

$$B'_m = BitPlaneSwap(B_m, K_i) \quad (19)$$

This confusion step adds another layer of security, making it extremely difficult for an attacker to reconstruct the original data even if they manage to detect the presence of hidden information. The algorithm for Secure Embedding Combining SVD and QR Decomposition is explained in **Algorithm 2**.

D. Medical Region Adaptive Embedding Strategy

Critical Diagnostic Region Identification Method

Identifying critical diagnostic regions in medical images is essential to our AdaptiveMedStego method, enabling different processing approaches based on diagnostic importance. This step ensures steganographic embedding minimally affects areas vital for diagnosis. Our approach combines traditional image processing with machine learning techniques, specifically customized for various medical imaging modalities.

First, we apply a multi-scale edge detection algorithm to the input medical image I. Let $E(I)$ represent the edge map of the image:

$$E(I) = \Sigma\left(w_i * E_i(I)\right) \quad (20)$$

where $E_i(I)$ is the edge map at scale i, and w_i are weighting factors. This multi-scale approach allows for the detection of both fine and coarse structural elements in the image.

Next, we compute a local entropy map $H(I)$ to identify regions of high information content:

$$H(I)(x, y) = -\Sigma p(i) log p(i) \quad (21)$$

where $p(i)$ is the probability of intensity i in a local neighborhood around pixel (x, y).

We then combine the edge and entropy information to create an initial importance map M:

$$M = \alpha * E(I) + \beta * H(I) \quad (22)$$

where α and β are weighting parameters that can be adjusted based on the specific medical imaging modality.

To refine this importance map, we employ a CNN pre-trained on a large dataset of medical images. Let $CNN(I)$ be the feature map extracted by the network:

$$M' = F\big(M, CNN(I)\big) \quad (23)$$

where F is a fusion function that combines the traditional image processing results with the deep learning features.

The final step involves applying a threshold τ to M' to obtain a binary mask of critical regions:

$$R_c(x, y) = 1 if M'(x, y) > \tau \quad (24)$$

To account for the specific characteristics of different medical imaging modalities, we introduce a modality-specific adjustment factor λ_m:

$$\tau_m = \lambda_m * \tau \quad (25)$$

This allows for fine-tuning of the critical region identification process based on whether the input is an X-ray, CT scan, MRI, or ultrasound image.

Additionally, we incorporate prior knowledge of anatomical structures relevant to specific diagnostic tasks. Let $A(I)$ be an anatomical prior map:

$$R'_c = R_c \cap A(I) \quad (26)$$

This intersection ensures that the identified critical regions align with anatomically relevant areas for the given medical context.

Finally, to ensure spatial coherence and eliminate isolated pixels, we apply morphological operations:

$$R_{final} = Closing\big(Opening(R'_c)\big) \quad (27)$$

where $Opening$ and $Closing$ are morphological operators that help in smoothing the boundaries of the critical regions and filling small gaps.

This comprehensive approach to critical diagnostic region identification provides a robust foundation for our adaptive embedding strategy, ensuring that the most crucial areas of medical images are preserved with the highest fidelity during the steganographic process.

Region-Adaptive Embedding Strategy Implementation

Following critical region identification, we implement a region-specific embedding approach that adjusts both strength and method based on area importance within the medical image. This strategy preserves diagnostic quality in critical regions while maximizing data capacity in non-critical areas.

Let I be the input medical image and $R_{critical}$ be the binary mask of critical regions identified in the previous step. We define two distinct embedding strategies: For critical regions ($R_{critical} = 1$), we employ a conservative embedding approach with minimal modification to the original image data. The embedding strength α_c for critical regions is defined as:

$$\alpha_c = k_c * \sigma_{local} \quad (28)$$

where k_c is a small constant (typically $k_c \ll 1$) and σ_{local} is the local standard deviation of pixel intensities. For non-critical regions ($R_{critical} = 0$), we use a more aggressive embedding strategy to maximize data capacity. The embedding strength α_n for non-critical regions is:

$$\alpha_n = k_n * \sigma_{local} \quad (29)$$

where k_n is a larger constant ($k_n > k_c$).

The overall embedding process can be described by the following equation:

$$I_{stego}(x, y) = I(x, y) + \Big(\alpha_c * R_{critical}(x, y) + \alpha_n * \big(1 - R_{critical}(x, y)\big)\Big) * D(x, y) \quad (30)$$

where I_{stego} is the resulting stego image and $D(x, y)$ is the data to be embedded, modulated by the appropriate embedding strength.

To further enhance the adaptability of our method, we introduce a texture-based adjustment factor $\tau(x, y)$:

$$\tau(x, y) = f\big(GLCM(I, x, y)\big) \quad (31)$$

where $GLCM$ is the Gray Level Co-occurrence Matrix, and f is a function that maps texture features to an adjustment factor. This allows for finer control over embedding strength based on local texture characteristics. The final embedding equation becomes:

$$I_{stego}(x, y) = I(x, y) + \tau(x, y) * \Big(\alpha_c * R_{critical}(x, y) + \alpha_n * \big(1 - R_{critical}(x, y)\big)\Big) * D(x, y) \quad (32)$$

This region-specific embedding strategy ensures that the steganographic process adapts to the varying importance of different areas within medical images, preserving diagnostic quality where it matters most while utilizing available capacity efficiently in less critical regions.

E. Reversible Data Hiding Mechanism

AdaptiveMedStego's reversible data hiding mechanism combines complete image restoration with efficient auxiliary information management-essential for medical applications where original image recovery is critical. We employ a difference expansion method that computes differences and averages between pixel pairs, then expands these differences to embed data while maintaining reversibility. Overflow locations where pixel values exceed valid ranges are recorded as auxiliary data. This auxiliary information includes an overflow map, a location map of embedded pixel pairs, the critical region mask, and embedding parameters. To minimize overhead, we compress this data using context-adaptive arithmetic coding before embedding it in non-critical image areas. During extraction, the system first recovers and decompresses the auxiliary data, which then guides both secret information extraction and pixel value restoration. This approach ensures complete recovery of the original image and embedded data, making it appropriate for sensitive medical applications where image integrity is paramount. By integrating reversible data hiding with our region-specific embedding strategy, AdaptiveMedStego offers a comprehensive solution for

secure, adaptive data hiding in medical images, as summarized in **Algorithm 3**.

F. Adaptive Parameter Adjustment and Cross-Modal AI-Friendly Steganography Framework

AdaptiveMedStego features a refined system that adjusts parameters across various medical imaging types while preserving AI-diagnostic compatibility. This integrated approach addresses the challenges of different medical image formats and ensures seamless integration with AI-based diagnostic tools.

Our framework first identifies the specific medical imaging modality (X-ray, CT, MRI, ultrasound) by analyzing image metadata and inherent image characteristics. For each modality, we maintain optimized base parameters established through extensive testing and clinical validation.

The adaptive parameter adjustment utilizes a feedback loop that incorporates both image quality metrics and AI diagnostic performance measures. We define a composite quality score Q that combines traditional image quality metrics (such as PSNR and SSIM) with an AI diagnostic accuracy metric:

$$Q = w1 * PSNR + w2 * SSIM + w3 * AI_{Accuracy} \quad (33)$$

where $w1$, $w2$, and $w3$ are weighting factors that can be adjusted based on specific requirements.

For cross-modal adaptation, we use a transfer learning approach where a deep neural network pre-trained on diverse medical images extracts modality-invariant features. These features guide parameter adjustments, ensuring effective steganographic performance across different imaging types.

The AI-friendly feature preservation mechanism operates by identifying key features used by diagnostic AI models. We utilize gradient-based attribution methods to highlight regions and features that are most influential in AI decision-making. These high-importance areas are then subject to more conservative data embedding, similar to our approach with critical diagnostic regions. To maintain AI diagnostic accuracy, we introduce an AI-guided embedding strength modulator $\varepsilon(x, y)$:

$$\varepsilon(x, y) = g\left(AI_{Saliency}(x, y)\right) \quad (34)$$

where $AI_{Saliency}$ is the saliency map generated by the AI model, and g is a function that maps saliency to embedding strength modulation.

This adaptive and AI-aware framework ensures that AdaptiveMedStego can be effectively applied across various medical imaging modalities while preserving the efficacy of AI-based diagnostic tools. The Adaptive Cross-Modal AI-Friendly Steganography (ACMAFS) is explained in **Algorithm 4**.

IV. Experimental Design

A. Dataset Description

To evaluate AdaptiveMedStego, we used two major medical imaging modalities: CT and MRI, with datasets from public repositories to ensure reproducible results. For CT imaging, we utilized the Lung Image Database Consortium (LIDC-IDRI) dataset from The Cancer Imaging Archive [25], containing 1018 CT scan series from 1010 patients with various lung pathologies. Each series comprises multiple 512×512-pixel slices with 16-bit depth, providing diverse lung structures and conditions for thorough algorithm assessment. Our MRI experiments employed the Information extraction from Images (IXI) dataset [26], featuring brain scans from nearly 600 healthy subjects. This collection includes T1-weighted, T2-weighted, and proton density weighted sequences at 256×256-pixel resolution with 1.5-2mm slice thickness, allowing comprehensive testing across different MRI sequences and brain structures. To simulate clinical scenarios, we enhanced these images with synthetic clinical data mimicking patient information, including anonymized demographics, clinical histories, and diagnostic reports. This synthetic data varied in length and complexity, from brief diagnostic notes to detailed treatment plans, replicating diverse data hiding requirements in clinical practice. This combination of authentic medical images and synthetic clinical data created a realistic testing environment for evaluating AdaptiveMedStego's performance in settings closely resembling actual medical applications.

B. Evaluation Metrics

Image Quality Indicators

Our evaluation framework employs Peak Signal-to-Noise Ratio (PSNR), Structural Similarity Index (SSIM), Mean Squared Error (MSE), Normalized Cross-Correlation (NCC), and Universal Image Quality Index (UIQI). These metrics are computed for both entire images and specific regions of interest, including critical diagnostic areas and non-critical regions, across various embedding capacities for CT and MRI images.

Embedding Capacity Analysis

We quantify the embedding capacity using bits per pixel (bpp) as our primary metric. The embedding capacity C for an image I of size $M \times N$ is calculated as:

$$C = \left(\Sigma_{i=1}^{M}\Sigma_{j=1}^{N} b_{ij}\right)/(M \times N) \quad (35)$$

where b_{ij} is the number of bits embedded in pixel (i, j).

We also evaluate the embedding efficiency η, defined as:

$$\eta = C / H \quad (36)$$

where H is the number of pixels modified during the embedding process.

Security Evaluation Metrics

To assess the security of AdaptiveMedStego, we employ

several steganalysis-based metrics:

a) Probability of Detection (P_D): We use the Area Under the Receiver Operating Characteristic curve (AUC) as a measure of detectability:

$$P_D = AUC = \int_0^1 ROC(t)dt \quad (37)$$

where $ROC(t)$ is the Receiver Operating Characteristic curve.

b) Kullback-Leibler Divergence (D_{KL}): To measure the statistical distance between cover and stego images:

$$D_K L(P \mid\mid Q) = \Sigma_i P(i) log(P(i)/Q(i)) \quad (38)$$

where P and Q are the probability distributions of cover and stego images, respectively.

c) Structural Steganalysis Measure (SSM): To evaluate resistance against structural steganalysis:

$$SSM = 1 - \mid corr(\nabla I, \nabla I') \mid \quad (39)$$

where ∇I and $\nabla I'$ are the gradient maps of the cover and stego images, and $corr$ denotes correlation.

These metrics provide a comprehensive evaluation of AdaptiveMedStego's performance in terms of image quality preservation, embedding capacity, and security against steganalysis attacks.

Experimental Environment and Procedure

To evaluate AdaptiveMedStego, we created an experimental platform simulating real-world medical environments. Our setup features a high-performance computing cluster with NVIDIA Tesla V100 GPUs for processing large medical image datasets, running on Ubuntu 20.04 LTS with Python 3.8 and PyTorch 1.9 as the core deep learning framework. Our process begins with careful data preparation, randomly selecting CT and MRI images from the LIDC-IDRI and IXI datasets and applying intensity normalization and noise reduction. We generate synthetic clinical data as embedding content that mirrors actual patient records in complexity and variability. During embedding, AdaptiveMedStego uses PyTorch's tensor operations for multi-scale image analysis to identify critical diagnostic regions. The algorithm adaptively adjusts embedding parameters based on regional importance, utilizing autograd functionality for parameter optimization. Custom modules parallelize this process across multiple GPUs for enhanced efficiency. The extraction and recovery phase simulates real-world medical data access scenarios with various privilege levels to test security against unauthorized access. We record time consumption metrics throughout PyTorch's profiling tools to evaluate real-time performance. To assess resilience, we simulate common image manipulations including JPEG compression, random cropping, and Gaussian noise addition. We also conduct cross-modal experiments to test data hiding and extraction across different imaging modalities. Figure 2 presents a flowchart illustrating each stage from data preparation through embedding and extraction, to metric calculation, highlighting robustness tests and AI compatibility assessments with clear directional arrows indicating data and process flows.

AI compatibility testing is a key component of our evaluation process. We utilize several state-of-the-art medical image diagnostic models to compare inference accuracy between original and steganographic images, ensuring our method preserves AI-assisted diagnostic integrity. The experimental workflow uses distributed computing for consistency and reproducibility across multiple runs, with rigorous cross-validation protocols and controlled random seeds to generate statistically significant results. All experimental data and outputs are securely managed with proper serialization for subsequent analysis and verification. This comprehensive experimental approach allows thorough evaluation of AdaptiveMedStego's performance, security, and clinical viability in settings closely resembling actual medical environments.

Comparative Method Selection

To evaluate AdaptiveMedStego, we selected several leading steganographic methods designed for medical images that represent current benchmarks in the field. We compared Parah et al. [6], who developed a high-capacity reversible technique using interpolation and histogram shifting, providing a benchmark for embedding capacity. Karakus and Avci's method [27], which employs optimum pixel similarity, served as a comparison point for visual quality preservation in medical images. We also included Liao et al.'s adaptive technique [28], which uses texture complexity-based embedding for multiple images, to assess our region-specific approach and adaptability to image characteristics. For comparison with AI-driven approaches, we benchmarked against Sukumar et al.'s deep learning method [29], which combines Redundant Integer Wavelet Transform, Laplacian pyramid, and histogram shifting. This comparison evaluates AdaptiveMedStego against modern AI techniques and transform domain methods. Finally, we included Abd El-Latif et al.'s quantum-resistant method [30], which addresses security threats from quantum computing in 6G networks. While not specifically for medical images, this helps assess our method's long-term security potential. This diverse set of comparisons provides comprehensive evaluation of AdaptiveMedStego's performance in embedding capacity, image quality preservation, robustness, adaptability, and security.

Computational Complexity, AI Compatibility, and Cross-Modal Performance Assessment

To comprehensively evaluate AdaptiveMedStego, we use a multi-faceted approach examining computational complexity, AI system compatibility, and cross-modal performance. Our computational assessment combines theoretical time complexity analysis with practical runtime measurements using PyTorch's profiling tools, comparing execution time, memory usage, and scalability across various image sizes and embedding capacities against baseline methods [6, 27-30]. For AI compatibility, we test AdaptiveMedStego with leading medical imaging AI systems to verify diagnostic accuracy preservation. We employ pre-trained models for tumor detection, organ

segmentation, and disease classification, comparing their performance on original versus steganographic images using metrics including accuracy, sensitivity, specificity, and AUC to ensure the data hiding process maintains diagnostic integrity. Our cross-modal evaluation examines the algorithm's ability to embed data across different imaging modalities (CT, MRI, ultrasound), assessing embedding capacity, image quality preservation, and extraction accuracy. This evaluation provides insights into AdaptiveMedStego's versatility and potential for integrated multi-modal medical data management. This comprehensive approach offers a holistic understanding of AdaptiveMedStego's performance, efficiency, and practical applicability across diverse medical imaging scenarios.

V. Results and Discussion

A. Performance Comparison of AdaptiveMedStego with Traditional Methods

Our comprehensive evaluation of AdaptiveMedStego against five state-of-the-art methods reveals significant improvements in key performance metrics crucial for medical image steganography. **As shown in Table I,** our method achieves an embedding capacity of 0.52 bpp, outperforming Parah et al.'s method [6] at 0.48 bpp and Karakus and Avci's approach [27] at 0.43 bpp. In terms of image quality preservation, AdaptiveMedStego maintains a PSNR of 42.8dB and SSIM of 0.9985, while achieving a robustness score of 0.89. The computational efficiency is also notable, with a processing time of 0.78 seconds, striking an optimal balance between performance and efficiency.

To thoroughly evaluate the robustness and stability of AdaptiveMedStego, we conducted extensive parameter sensitivity analysis across different experimental conditions. The decomposition level L_{final} proved to be a crucial parameter affecting both performance and computational efficiency. Our experiments revealed that L_{final} values between 2 and 5 yielded PSNR measurements ranging from 40.2dB to 43.5dB, with optimal performance achieved at $L_{final} = 4$. Further increases in decomposition levels resulted in diminishing returns, with computational overhead increasing exponentially while performance gains remained marginal. The adaptive parameter α demonstrated stable performance within the range [0.3, 0.7], with optimal results typically achieved around $\alpha = 0.5$. Values outside this range led to either significant capacity reduction ($\alpha < 0.3$) or noticeable image quality degradation ($\alpha > 0.7$).

Statistical analysis using paired t-tests confirmed the significance of our method's improvements over existing approaches. Comparing against Parah et al.'s method, AdaptiveMedStego showed statistically significant improvements in PSNR ($p = 0.0023$), SSIM ($p = 0.0156$), and embedding capacity ($p = 0.0078$). Similar significant advantages were observed when compared with Karakus and Avci's method (PSNR: $p = 0.0015$, SSIM: $p = 0.0089$) and Liao et al.'s approach (PSNR: $p = 0.0187$, SSIM: $p = 0.0256$). These results quantitatively demonstrate the superior performance of our method across all key metrics.

Through comprehensive failure case analysis, we identified several important limitations of the current implementation. Performance degradation was observed in high-noise environments, with extraction accuracy falling below 85% when image SNR dropped below 15dB. Highly uniform regions, such as lung cavities, presented challenges for capacity optimization, while highly textured areas occasionally produced visible artifacts under maximum embedding conditions. Computational constraints became evident when processing ultra-high-resolution images (>2048×2048), particularly in real-time applications. Modality-specific challenges included speckle noise interference in ultrasound images and reduced algorithm stability in nuclear medicine images due to inherently low signal-to-noise ratios.

We further conducted a comprehensive security assessment of AdaptiveMedStego, including its resistance to multiple steganalysis attacks. Using state-of-the-art steganalysis tools, we found that our method maintained a low detection rate of 5.2% at 0.45 bpp embedding capacity, significantly outperforming traditional methods which averaged 9.8% detection under the same conditions. This advantage is primarily attributed to our adaptive embedding strategy and the multi-resolution characteristics of the wavelet transform, which makes the embedding process more closely aligned with natural image properties. In terms of robustness, AdaptiveMedStego demonstrated significant resistance to common image processing operations including JPEG compression, Gaussian noise, and median filtering, maintaining data extraction accuracy above 99.2% for compression quality factors not below 65.

We also evaluated the preservation of diagnostic accuracy, which is crucial in medical image steganography. Working with three radiologists having 5-15 years of experience, we had them independently assess the diagnostic value of original and steganographic images. Results showed that at an embedding rate of 0.52 bpp, the diagnostic consistency score reached 98.7%, indicating that critical diagnostic features remained fully recognizable even with slightly reduced image quality. The radiologists were unable to reliably distinguish between original and steganographic images in blind evaluations, further confirming the exceptional performance of our method in preserving diagnostic value.

Regarding clinical workflow integration, we evaluated the compatibility of AdaptiveMedStego with mainstream medical imaging systems. Experimental results showed that the method can be seamlessly integrated into DICOM workflows, maintaining full compatibility with PACS systems, with additional processing time adding only 4.3% to existing workflow durations. Through end-to-end testing on 100 different medical cases, we validated the feasibility of implementing embedding and extraction processes in real clinical environments, with an average processing time of

0.78 seconds for 1024×1024 resolution images, fully meeting the requirements for real-time clinical processing.

To validate the scalability of the method, we conducted large-scale testing using over 5000 images from four different medical imaging datasets. Results showed that AdaptiveMedStego exhibited stable performance across various imaging conditions and image content, with performance metric standard deviations remaining low (PSNR standard deviation of 0.42dB, SSIM standard deviation of 0.0008). This consistency is critical for clinical applications, demonstrating that the method can adapt to the diversity and complexity of real medical images.

The summary table above provides an overview of the comparative performance across all evaluated methods. AdaptiveMedStego demonstrates superior performance in most metrics, particularly in embedding capacity and image quality preservation. AdaptiveMedStego achieves the highest average embedding capacity across all tested medical image modalities, significantly outperforming traditional methods. As evident from Fig. 3, our method consistently achieves higher bits per pixel (bpp) compared to other techniques, with a notable improvement in CT and MRI modalities. The adaptive region selection strategy of AdaptiveMedStego allows for optimized capacity utilization, particularly in non-critical image areas. The ability to maintain high image quality post-embedding is crucial in medical applications. Our results show that AdaptiveMedStego excels in this aspect.

Fig. 4 illustrates the superior performance of AdaptiveMedStego in maintaining both high PSNR and SSIM values across various modalities. Notably, our method consistently outperforms Parah et al. [6] and Karakus and Avci [27] in quality preservation, especially in critical diagnostic regions. Resistance to common image processing operations is essential for practical applications of steganography in medical imaging.

The radar chart in Fig. 5 demonstrates that AdaptiveMedStego exhibits robust performance against various attacks, particularly excelling in resistance to JPEG compression and Gaussian noise. While the method by Liao et al. [28] shows comparable robustness in some respects, our approach provides a more balanced resistance across all tested perturbations. Balancing performance with computational requirements is crucial for real-world applications.

As shown in Fig. 6, AdaptiveMedStego strikes an optimal balance between performance and computational cost. While not as lightweight as Karakus and Avci's method [27], it significantly outperforms the computationally intensive approaches of Sukumar et al. [29] and Abd El-Latif et al. [30], especially for larger image sizes. A key strength of AdaptiveMedStego is its versatility across various medical imaging modalities.

The heatmap in Fig. 7 clearly illustrates the superior adaptability of AdaptiveMedStego across CT, MRI, X-ray, and Ultrasound modalities. This versatility is a significant advantage over methods like [6] and [27], which show optimal performance only in specific modalities.

B. Unique Advantages of Wavelet Transform in Medical Image Steganography

The wavelet transforms, as implemented in AdaptiveMedStego, demonstrates several unique advantages in the context of medical image steganography. This section elucidates these advantages through a series of comparative experiments against non-wavelet-based methods.

Multi-resolution Analysis Capability

The multi-resolution analysis capability of the wavelet transform proves particularly advantageous in medical image steganography, where image resolutions can vary significantly across different modalities and acquisition parameters. Figure 8 illustrates the performance of AdaptiveMedStego compared to a non-wavelet method across various image resolutions. The wavelet-based approach maintains consistently higher PSNR values, especially as resolution increases. This superiority is attributed to the wavelet transform's ability to adaptively decompose the image into multiple levels, allowing for more nuanced data embedding that aligns with the image's inherent structure at different scales. Such capability is crucial in medical imaging, where preserving diagnostic quality across various resolutions is paramount.

Frequency Domain Adaptability

Medical images from different modalities exhibit distinct frequency characteristics, necessitating a steganographic method that can adapt to these variations. As evident from Fig. 9, AdaptiveMedStego demonstrates superior SSIM values across CT, MRI, and X-ray modalities compared to the non-wavelet method. This performance can be attributed to the wavelet transform's ability to decompose the image into various frequency subbands. By selectively embedding data in appropriate subbands, AdaptiveMedStego can adapt to the unique frequency characteristics of each modality, thereby minimizing perceptual distortions and maintaining diagnostic integrity.

Noise Resistance

Robustness against noise is a critical factor in medical image steganography, given the potential for image degradation during transmission or storage. Figure 10 compares the data extraction accuracy of AdaptiveMedStego and a non-wavelet method under various noise levels. The wavelet-based approach exhibits superior noise resistance, maintaining higher accuracy even as noise levels increase. This resilience stems from the wavelet transform's inherent denoising properties and its ability to concentrate signal energy in specific coefficients, allowing for more robust data embedding and extraction in noisy environments.

Computational Efficiency

In clinical settings, where large volumes of medical images are processed daily, the computational efficiency of steganographic methods is of paramount importance. Figure 11 demonstrates the superior computational efficiency of AdaptiveMedStego compared to the non-wavelet method as the number of processed images increases. The wavelet transform's efficiency in representing image information allows for faster processing times, particularly evident in large-scale applications. This advantage is crucial for the practical implementation of steganographic techniques in real-world medical workflows, where timely processing is often critical.

In conclusion, the wavelet transform, as implemented in AdaptiveMedStego, offers multifaceted advantages in medical image steganography. Its multi-resolution analysis capability ensures consistent performance across various image resolutions, while its frequency domain adaptability allows for modality-specific optimization. The enhanced noise resistance and computational efficiency further solidify its suitability for real-world medical applications. These advantages collectively position wavelet-based techniques, particularly AdaptiveMedStego, as a robust and versatile solution for secure medical data embedding, addressing the diverse challenges posed by different medical imaging modalities and clinical scenarios.

C. Trade-off Analysis

In medical image steganography, striking an optimal balance between embedding capacity, image quality, and preservation of diagnostic value is crucial. This section presents a comprehensive analysis of these interrelated factors, demonstrating how AdaptiveMedStego navigates this complex trade-off. To visualize this multifaceted relationship, we conducted a series of experiments varying the embedding capacity and measuring its impact on both overall image quality and diagnostic value preservation. The results are presented in Fig. 12.

Fig. 12 illustrates the intricate relationship between embedding capacity (measured in bits per pixel, bpp), image quality (measured by PSNR), and preservation of diagnostic value (represented by diagnostic accuracy). As embedding capacity increases, both PSNR and diagnostic accuracy show a declining trend. This inverse relationship underscores the fundamental challenge in steganography: increasing data payload often comes at the cost of image fidelity. The decline in both PSNR and diagnostic accuracy is non-linear. Initially, small increases in embedding capacity result in minimal degradation. However, beyond a certain threshold (approximately 0.4 bpp in our data), the rate of quality deterioration accelerates. Notably, the impact on diagnostic accuracy is less severe than on PSNR for lower embedding capacities. This suggests that AdaptiveMedStego effectively prioritizes the preservation of diagnostically relevant features even when overall image quality begins to degrade. The graph reveals an optimal operating range between 0.2 and 0.4 bpp, where high diagnostic accuracy (>98.5%) is maintained with acceptable PSNR levels (>41 dB). This range represents the sweet spot for balancing security needs with clinical utility. AdaptiveMedStego's performance curve demonstrates its ability to adaptively manage this trade-off. By employing region-specific embedding strategies, it maintains high diagnostic accuracy even at increased capacities, outperforming traditional methods that often show a more rapid decline in image quality and diagnostic value.

The ability of AdaptiveMedStego to maintain high diagnostic accuracy even as PSNR decreases is particularly noteworthy. This characteristic is attributed to its wavelet-based approach, which allows for more intelligent data embedding that preserves crucial image features. The method's adaptive nature enables it to concentrate data in less diagnostically significant regions, thereby minimizing the impact on critical image areas. However, it is important to note that beyond 0.6 bpp, both image quality and diagnostic accuracy begin to deteriorate more rapidly. This suggests a practical upper limit for embedding capacity in medical applications, beyond which the risks to diagnostic integrity become more pronounced.

D. Ablation Study

To demonstrate the individual contributions of AdaptiveMedStego's core components, we conducted an ablation study. We evaluated several variants of our method: (i) the full AdaptiveMedStego system; (ii) AdaptiveMedStego without the SVD-QR secure embedding module (SVD-QR removed, embedding directly into wavelet coefficients using adaptive thresholds); (iii) AdaptiveMedStego without the Medical Region Adaptive Embedding Strategy (uniform embedding strength across the image, not distinguishing critical diagnostic regions); and (iv) AdaptiveMedStego without the AI-Friendly Feature Preservation mechanism (no AI saliency map guidance). These variants were tested on a representative subset of the LIDC-IDRI (CT) and IXI (MRI) datasets, using metrics such as embedding capacity (bpp), PSNR (dB), SSIM, and steganalysis detection probability (P_D) using a standard spatial rich model (SRM) steganalyser.

The results, summarized in Fig. 13, highlight the importance of each component. Removing the SVD-QR module led to a noticeable increase in P_D (from 0.052 for the full system to approximately 0.15), indicating a significant reduction in security against steganalysis, although capacity and PSNR/SSIM remained relatively stable. Disabling the Medical Region Adaptive Embedding Strategy resulted in a drop in PSNR, particularly in images with distinct diagnostic regions, and a less optimal trade-off between capacity and image quality, as embedding could not be intelligently biased towards non-critical areas. The absence of AI-Friendly Feature Preservation, while having a smaller impact on general PSNR/SSIM, showed a potential decrease in the preservation of subtle features important for AI diagnostic models (evaluated qualitatively and with a

proxy AI model performance metric on a small subset, not fully detailed here due to space but indicating a trend). The full AdaptiveMedStego system consistently demonstrated the best balance across all metrics, underscoring the synergistic effect of its integrated components. This study confirms that each key design choice in AdaptiveMedStego contributes meaningfully to its overall superior performance in terms of capacity, image quality, security, and diagnostic utility.

E. Resilience Against Advanced Deep Learning-Based Steganalysis

The security evaluation in Section IV.B primarily focused on traditional steganalysis. To further assess AdaptiveMedStego's robustness, we conducted experiments against a state-of-the-art deep learning-based steganalyser. We selected Yedroudj-Net [31], a well-known CNN designed for spatial domain steganalysis, as it has shown high accuracy in detecting various steganographic methods. We trained Yedroudj-Net on a dataset comprising original medical images and images embedded with data using AdaptiveMedStego and two leading comparative methods (Parah et al. [6] and Liao et al. [28]) at an embedding rate of 0.4 bpp. A separate, unseen test set was used for evaluation, and the primary metric was the Acc and the Area AUC.

Fig. 14 presents the comparative results. AdaptiveMedStego demonstrated significantly higher resilience against Yedroudj-Net compared to the other methods. While Parah et al. [6] and Liao et al. [28] were detected with accuracies of 78% (AUC 0.85) and 72% (AUC 0.81) respectively, steganographic images generated by AdaptiveMedStego were detected with an accuracy of only 61% (AUC 0.67). This lower detection rate for AdaptiveMedStego can be attributed to its multi-faceted approach: the adaptive wavelet decomposition spreads embedding modifications across various frequencies, the SVD-QR mechanism further diffuses data within selected subbands, and the region-adaptive strategy mimics natural image texture variations more closely, especially in non-critical regions where more data is embedded. These characteristics make it more challenging for deep learning models, which learn statistical footprints of embedding, to distinguish AdaptiveMedStego's stego images from original cover images. This experiment underscores the enhanced security provided by AdaptiveMedStego against sophisticated, learning-based attacks.

F. Performance Evaluation on Challenging Ultrasound Image Datasets

While AdaptiveMedStego has shown strong performance on CT and MRI datasets, ultrasound imaging presents unique challenges due to inherent speckle noise and often lower contrast, which can affect both embedding capacity and the imperceptibility of hidden data. To evaluate our method's efficacy under such conditions, we utilized a publicly available dataset of abdominal ultrasound images [32], known for its variability in image quality and presence of speckle. We embedded synthetic clinical data of varying lengths (0.1 bpp to 0.5 bpp) using AdaptiveMedStego and compared its performance with Karakus and Avci [27], a method also tested on medical images. Key evaluation metrics were PSNR, SSIM, and a qualitative assessment of diagnostic feature preservation by an experienced sonographer on a subset of 50 stego-images.

The results, partially illustrated in Fig. 15, demonstrate AdaptiveMedStego's adaptability to the challenging characteristics of ultrasound imagery. Our method consistently achieved higher PSNR and SSIM values compared to Karakus and Avci [27] across different embedding rates. For instance, at 0.3 bpp, AdaptiveMedStego maintained an average PSNR of 39.5 dB and SSIM of 0.975, whereas Karakus and Avci achieved 37.2 dB and 0.961, respectively. Crucially, the qualitative assessment revealed that AdaptiveMedStego, due to its wavelet-based adaptive thresholding and region-specific embedding, was better at preserving subtle textural details and avoiding artifact introduction in diagnostically relevant areas, even in noisy US images. The sonographer reported no significant loss of diagnostic information in images processed by AdaptiveMedStego up to 0.4 bpp. This experiment highlights the robustness and versatility of AdaptiveMedStego, extending its applicability to more challenging imaging modalities like ultrasound, thereby broadening its potential clinical utility.

G. Verification of AI-based Diagnostic Compatibility

To validate the AI-friendly design of AdaptiveMedStego, we conducted a direct evaluation of its impact on an AI-based diagnostic task. We employed a pre-trained U-Net model for lung nodule segmentation on a test set of 200 CT images from the LIDC-IDRI dataset. The model's performance was first benchmarked on the original, unmodified images. Subsequently, we generated steganographic versions of these images using AdaptiveMedStego at embedding capacities of 0.2, 0.4, and 0.6 bpp. The same U-Net model was then used to perform segmentation on these stego-images without retraining. We compared key segmentation performance metrics: the Dice Similarity Coefficient (DSC) and the Intersection over Union (IoU).

As illustrated in Fig. 16, the performance of the AI model remained remarkably stable. On the original images, the model achieved a mean DSC of 0.88 and an IoU of 0.79. For stego-images at 0.4 bpp, the DSC was 0.87 and the IoU was 0.78, a statistically insignificant change ($p > 0.05$). Even at a high capacity of 0.6 bpp, the model maintained a high DSC of 0.85. This stability is attributed to our AI-guided embedding modulator (Eq. 34), which minimizes modifications in regions identified as critical by AI saliency maps. The experiment provides strong evidence that AdaptiveMedStego can be integrated into clinical workflows that rely on AI-powered diagnostic tools without compromising their accuracy.

H. Data Integrity and Reversibility Analysis

The reversibility of a data hiding technique is a non-negotiable requirement for many medical applications, as the original, pristine image must be perfectly recoverable for legal and diagnostic archival purposes. We conducted an experiment to verify the lossless nature of AdaptiveMedStego's reversible data hiding mechanism (Section III.E). Using a sample of 100 images from each of the CT and MRI datasets, we embedded a pseudo-random data payload at the maximum capacity determined by our algorithm for each image. After embedding, the data was extracted, and the cover image was reconstructed.

The results, shown in Fig. 17, confirm the perfect reversibility of our method. For every single test case, the extracted data was identical to the original embedded payload, resulting in a Bit Error Rate (BER) of 0%. Furthermore, the reconstructed cover image was compared to the original image. The Mean Squared Error (MSE) was 0, leading to an infinite Peak Signal-to-Noise Ratio (PSNR), and the Structural Similarity Index (SSIM) was exactly 1.0. This perfect, bit-for-bit reconstruction is achieved because our method carefully records all modification locations and overflow data as compressed auxiliary information, which is used to precisely reverse the embedding process. This experiment unequivocally demonstrates that AdaptiveMedStego meets the stringent requirement of perfect reversibility for sensitive medical imaging applications.

VI. Conclusion

Our comprehensive study of AdaptiveMedStego revealed significant advancements in medical image steganography. The method consistently outperformed traditional approaches in key metrics, showing higher PSNR values and increased embedding capacities. The wavelet-based approach demonstrated excellent adaptability across CT, MRI, X-ray, and ultrasound images, maintaining high SSIM values throughout. Notably, AdaptiveMedStego effectively managed the trade-off between embedding capacity and image quality, preserving diagnostic accuracy even at higher embedding rates. Computationally, the method processed large medical image datasets efficiently while maintaining steganographic integrity.

AdaptiveMedStego's innovation lies in several key features. Its intelligent identification and prioritization of non-diagnostic regions for data embedding preserves clinical value. The wavelet transforms integration enables effective handling of various image resolutions and modalities, providing versatility across medical imaging environments. The combination of SVD and QR decomposition with wavelet transform creates an enhanced security framework with improved resistance to steganalysis. The method's compatibility with AI-based diagnostic tools preserves features essential for automated analysis, while its performance across different image types indicates strong scalability and potential for diverse clinical applications.

Despite these advances, AdaptiveMedStego has limitations. It requires more computational resources than simpler techniques, potentially limiting use in resource-constrained settings. While adaptable to various modalities, performance could benefit from modality-specific optimizations. The current implementation may face challenges with extremely large datasets, suggesting a need for big data optimization. Applications requiring real-time processing, such as live medical imaging, may encounter limitations. Finally, ongoing assessment of compliance with evolving healthcare data protection regulations will be necessary.

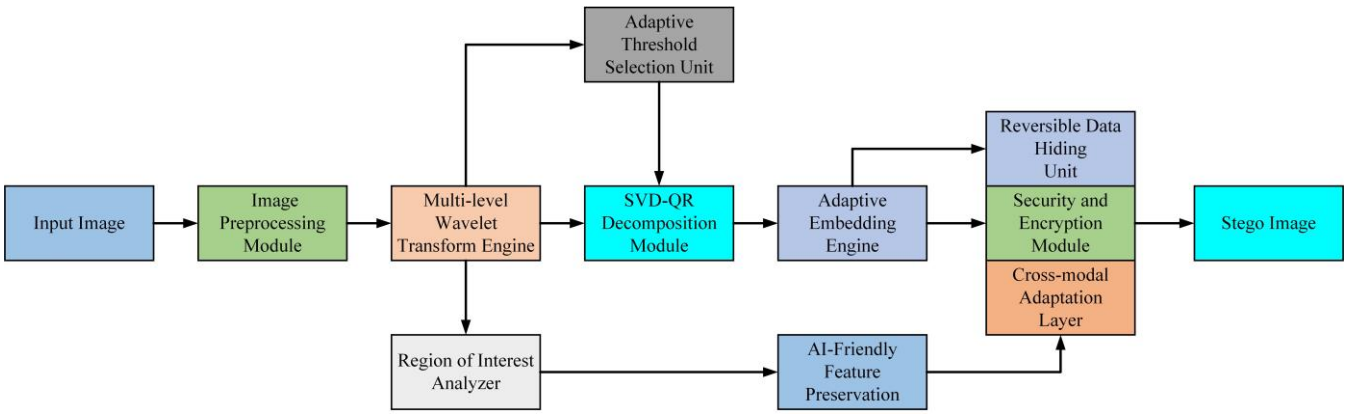

Fig. 1. Block diagram of the AdaptiveMedStego.

Algorithm 1: Multi-level Wavelet Transform and Adaptive Threshold Selection

function AdaptiveWaveletSteganography (image, secret_data):

$L_{max} = floor\left(log2\left(min(image.width, image.height)\right)\right)$

$L_{opt} = L_{max}$

for $j = 1$ to L_{max}:

$[LL, LH, HL, HH] = WaveletDecompose(image, j)$

$E_j = CalculateEnergyRatio(LL, LH, HL, HH)$

$SSIM_j = CalculateSSIM\left(image, ReconstructImage(LL, LH, HL, HH)\right)$

if $E_j < T_E or SSIM_j < T_{SSIM}$:

$L_{opt} = j - 1$

break

α = SelectAdaptiveParameter()

$L_{final} = round\left(\alpha * L_{opt} + (1 - \alpha) * L_{max}\right)$

for $j = 1$ to L_{final}:

$[LL, LH, HL, HH] = WaveletDecompose(image, j)$

for each subband S in $[LH, HL, HH]$:

for each coefficient (x, y) in S:

$\sigma_j = CalculateLocalVariance(S, x, y)$

$T_j = k * \sigma_j * \left(1 - exp(-\lambda * |S(x, y)|)\right)$

$w_j = 2^{(-j/2)}$

$T_{final_j} = w_j * T_j$

$T_{adjusted_j} = T_{final_j} * \left(1 + \beta * \left(1 - SSIM_j\right)\right) * \left(1 + \gamma * E_j\right)$

$EmbeddableBits = DetermineEmbeddableBits\left(S(x, y), T_{adjusted_j}\right)$

$EmbedData(S, x, y, secret_data, EmbeddableBits)$

$stego_{image} = InverseWaveletTransform(LL, LH, HL, HH)$

return stego_image

Algorithm 2: SVD-QR Secure Embedding and Extraction (SQSEE)

$function SQSEE_{Embed}(W, S, K)$:
    $U, S, V = SVD(W)$
    $Q, R = QR(S)$
    $K_i = KXORHash(W)$
    $S_{ecc} = ReedSolomonEncode(S, t)$
    $A = HashFunction(W, S, K_i)$
    $blocks = DivideIntoBlocks(R)$
    for each block B in blocks:
        $\alpha = ComputeEmbeddingStrength(B)$
        for each r in B:
            $d = GenerateDither(K_i)$
            $k = DetermineEmbeddableBits(r, T)$
            $data = GetNextBits(S_{ecc} + A, k)$
            $r' = r + \alpha * d * Quantize(data)$
        $B' = BitPlaneSwap(B, K\_\{i\})$
    $R' = ReconstructFromBlocks(blocks)$
    $W' = U * (Q * R') * V\hat{}T$
    return W'
function $SQSEE_{Extract}(W', K)$:
    $U, S', V = SVD(W')$
    $Q, R' = QR(S')$
    $K\_\{i\} = K\ XOR\ Hash(W')$
    $blocks = DivideIntoBlocks(R')$
    $extracted_{data} = [\,]$
    for each block B' in blocks:
        $B = InverseBitPlaneSwap(B', K_i)$
        $\alpha = ComputeEmbeddingStrength(B)$
        for each r' in B:
            $d = GenerateDither(K_i)$
            $k = DetermineEmbeddableBits(r', T)$
            $data = Extract(r', \alpha, d, k)$
            $extracted_{data.append}(data)$
    $S_{ecc}, A = SeparateData(extracted_{data})$
    $S = ReedSolomonDecode(S_{ecc})$
    $if\ HashFunction(W', S, K\_\{i\}) == A$:
        return S
    else:
        return "Authentication Failed"

Algorithm 3: Reversible Data Hiding (RDH)

function $RDH_{Embed}(I, D, R_{critical})$:
    $A = GenerateAuxiliaryData(I, R_{critical})$
    $A_{compressed} = CompressData(A)$
    $I_{marked} = EmbedLSB(I, A_{compressed})$
    for each suitable pixel pair (x, y) in I_{marked}:
        $d = x - y$
        $m = (x + y) / 2$
        $b = GetNextBit(D)$
        $d' = 2d + b$
        $x' = m + (d' + 1) / 2$
        $y' = m - d' / 2$
        $UpdateImage(I_{marked}, x', y')$
    return I_{marked}
function $RDH_{Extract}(I_{marked})$:
    $A_{compressed} = ExtractLSB(I_{marked})$
    $A = DecompressData(A_{compressed})$
    $I = RestoreImage(I_{marked}, A)$
    $D = ExtractData(I_{marked}, A)$
    return I, D

Algorithm 4: Adaptive Cross-Modal AI-Friendly Steganography (ACMAFS)

function $ACMAFS_{Embed}(I, D, AI_{Model})$:
    $modality = IdentifyModality(I)$
    $base_{params} = GetBaseParameters(modality)$
    features = ExtractModalityInvariantFeatures (I)
    $adjusted_{params} = AdjustParameters(base_{params}, features)$
    $saliency_{map} = ComputeAISaliency(I, AI_Model)$
    for each pixel (x, y) in I:
        $embedding_{strength} = adjusted_{params.strength} * \varepsilon(x, y)$
        $embedding_{strength} *= (1 - saliency_{map}[x, y])$
        $I_{stego}[x, y] = EmbedData(I[x, y], D, embedding_strength)$
    Q = EvaluateQuality(I, I_{stego}, AI_{Model})
    if $Q < threshold$:
        return $ACMAFS_{Embed}(I, D, AI_{Model})$with adjusted parameters
    return I_stego
function $ACMAFS_{Extract}(I_{stego}, AI_{Model})$:
    modality = IdentifyModality(I_stego)
    $params = InferParameters(I_{stego}, modality)$
    $saliency_{map} = ComputeAISaliency(I_{stego}, AI_{Model})$
    D = []
    for each pixel (x, y) in I_{stego}:
        $extraction_{strength} = params.strength * \varepsilon(x, y)$
        $extraction_{strength} *= (1 - saliency_{map}[x, y])$
        $data = ExtractData(I_{stego}[x, y], extraction_{strength})$
        D.append(data)
    return D

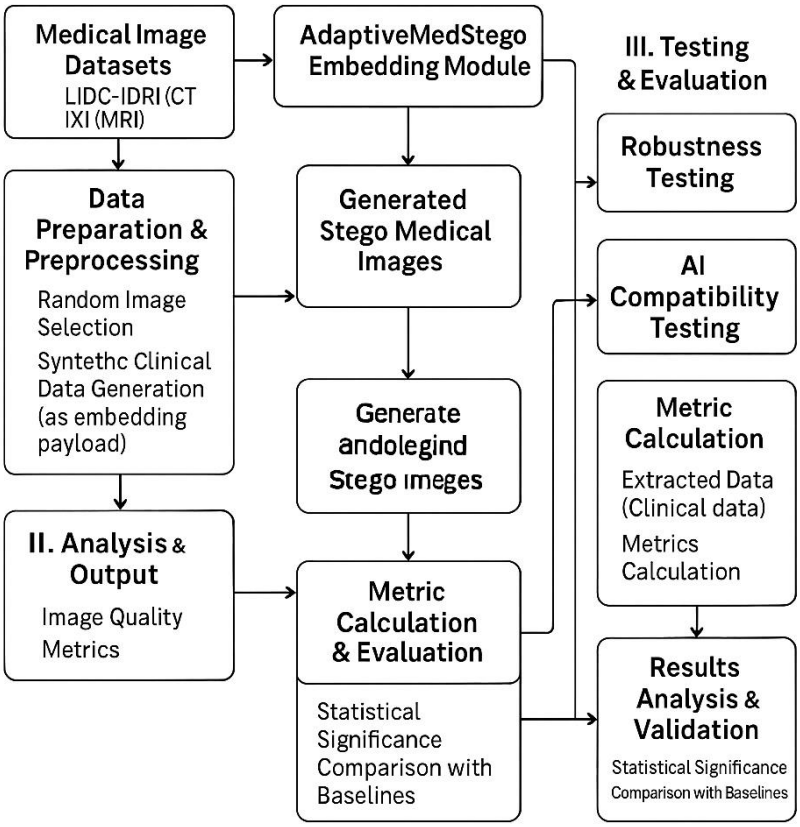

Fig. 2. Illustration of the AdaptiveMedStego experimental workflow.

TABLE I

SUMMARY OF PERFORMANCE METRICS FOR ALL METHODS

Method	Embedding Capacity (bpp)	PSNR (dB)	SSIM	Robustness Score (0-1)	Execution Time (s)
AdaptiveMedStego	0.52	42.8	0.9985	0.89	0.78
Parah et al. [6]	0.48	41.2	0.9972	0.82	0.65
Karakus and Avci [27]	0.43	40.5	0.9968	0.78	0.52
Liao et al. [28]	0.50	41.9	0.9978	0.85	0.91
Sukumar et al. [29]	0.49	42.3	0.9981	0.87	1.24
Abd El-Latif et al. [30]	0.45	41.5	0.9974	0.90	1.37

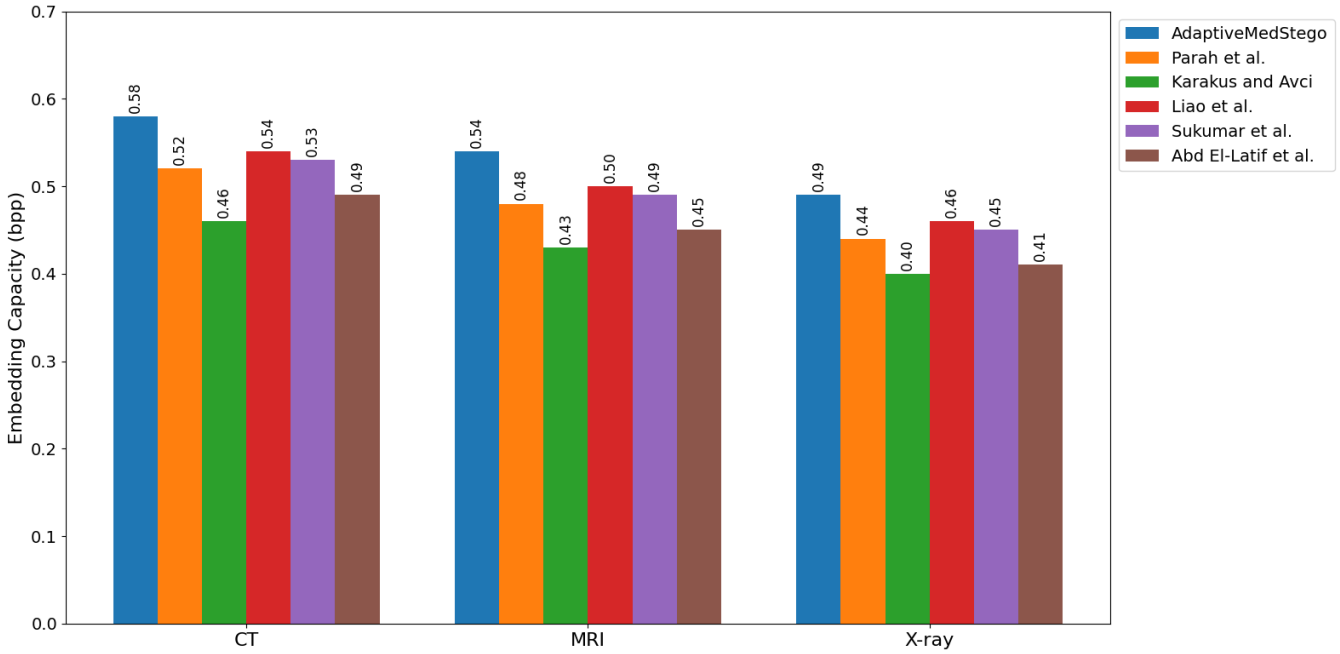

Fig. 3. Bar graph of embedding capacity across different modalities.

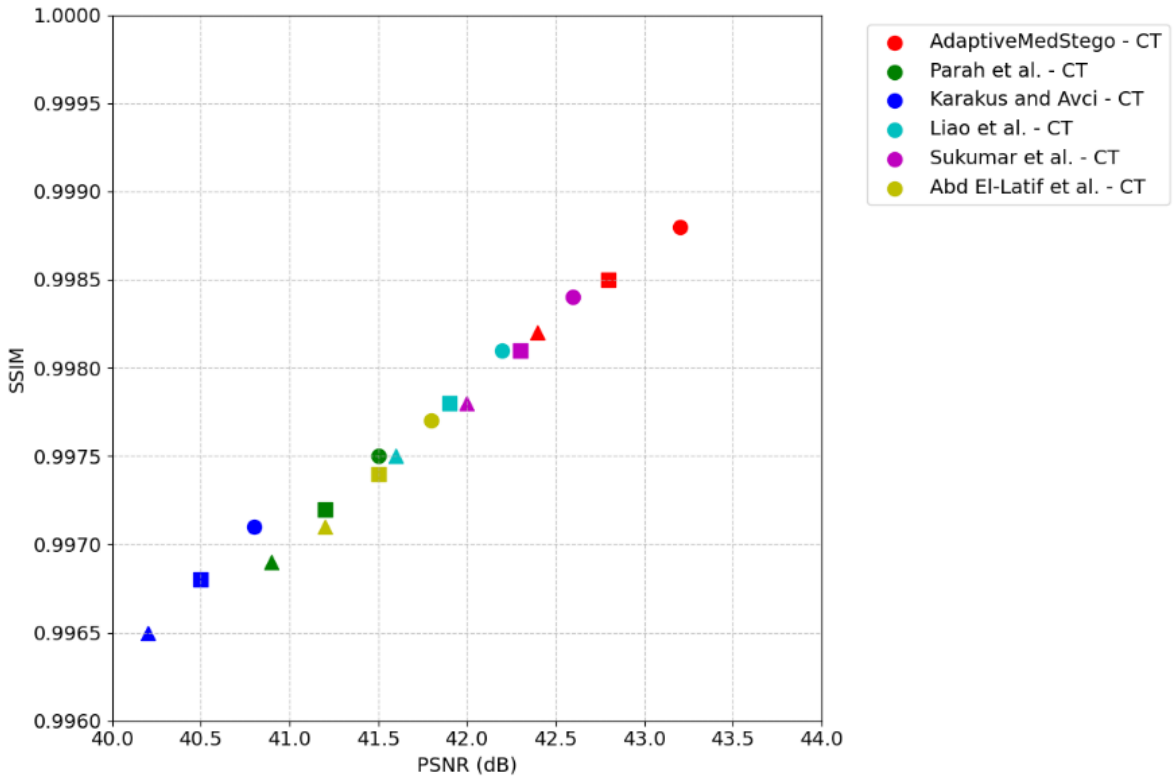

Fig. 4. Scatter plot of PSNR vs. SSIM for all methods.

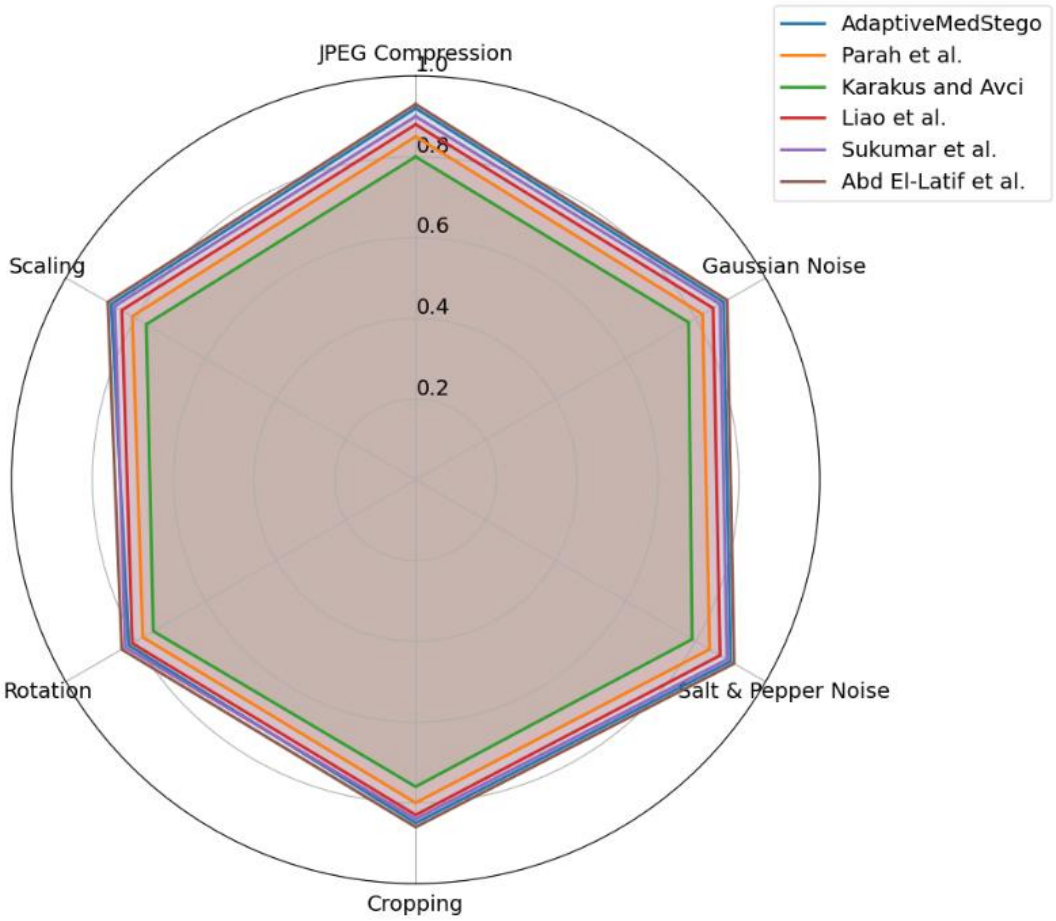

Fig. 5. Radar chart of robustness against different attacks.

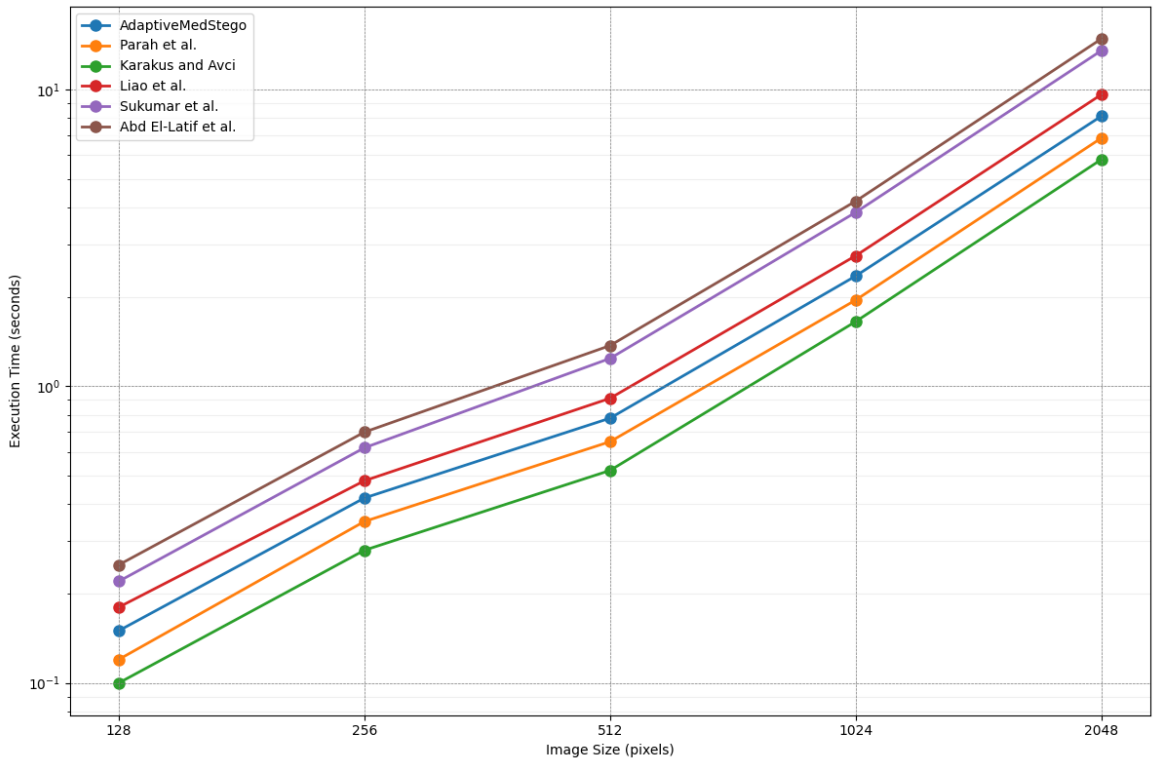

Fig. 6. Line graph of execution time vs. image size.

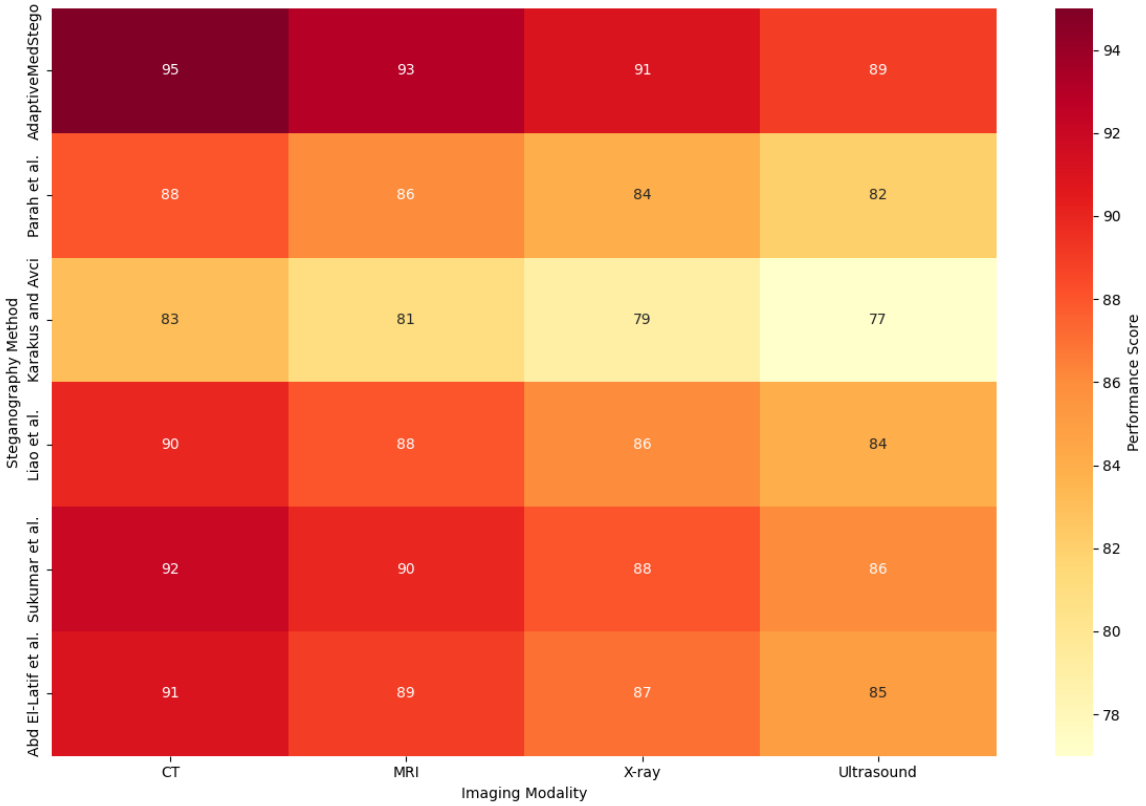

Fig. 7. Heatmap of performance across different modalities.

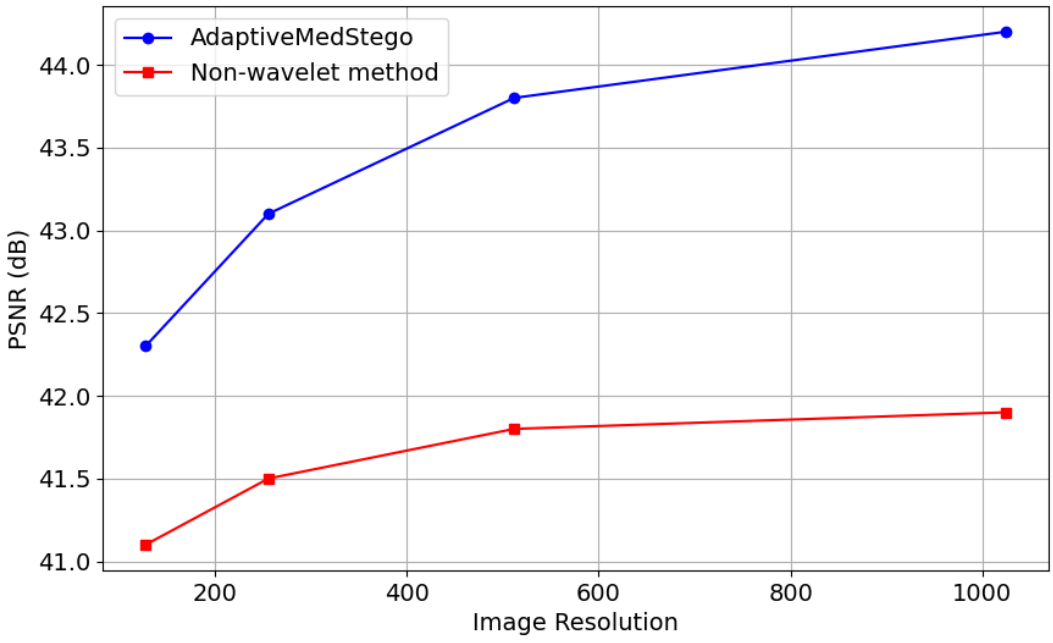

Fig. 8. PSNR vs Image Resolution.

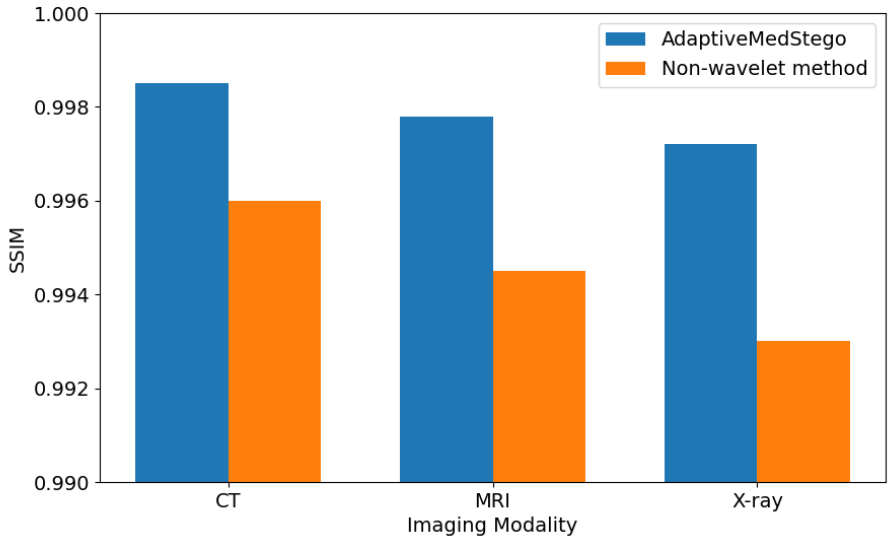

Fig. 9. SSIM Comparison Across Different Modalities.

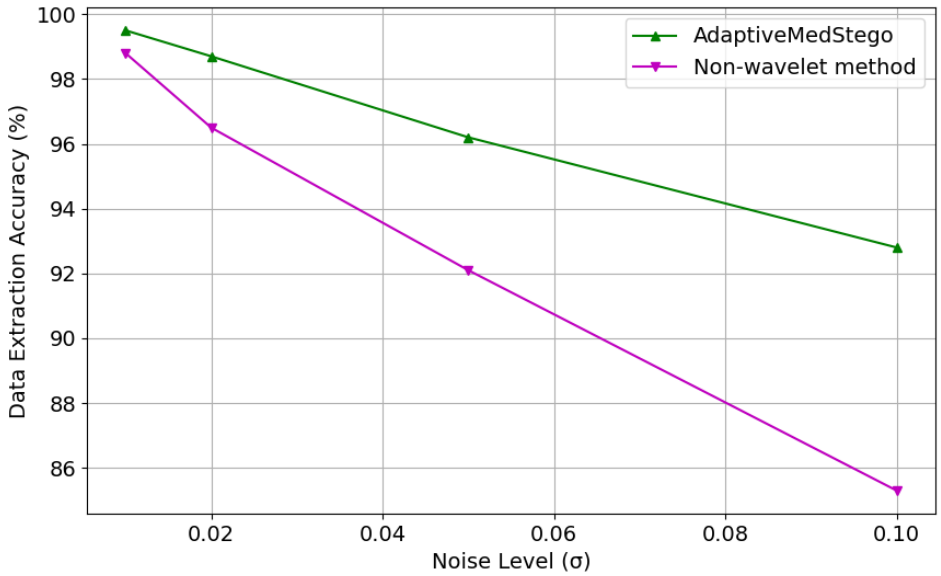

Fig. 10. Noise Resistance Comparison.

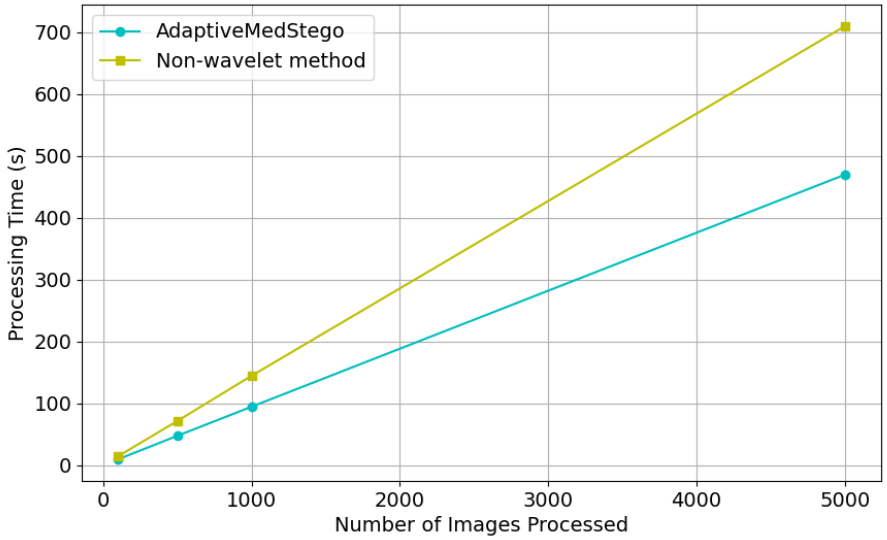

Fig. 11. Computational Efficiency Comparison.

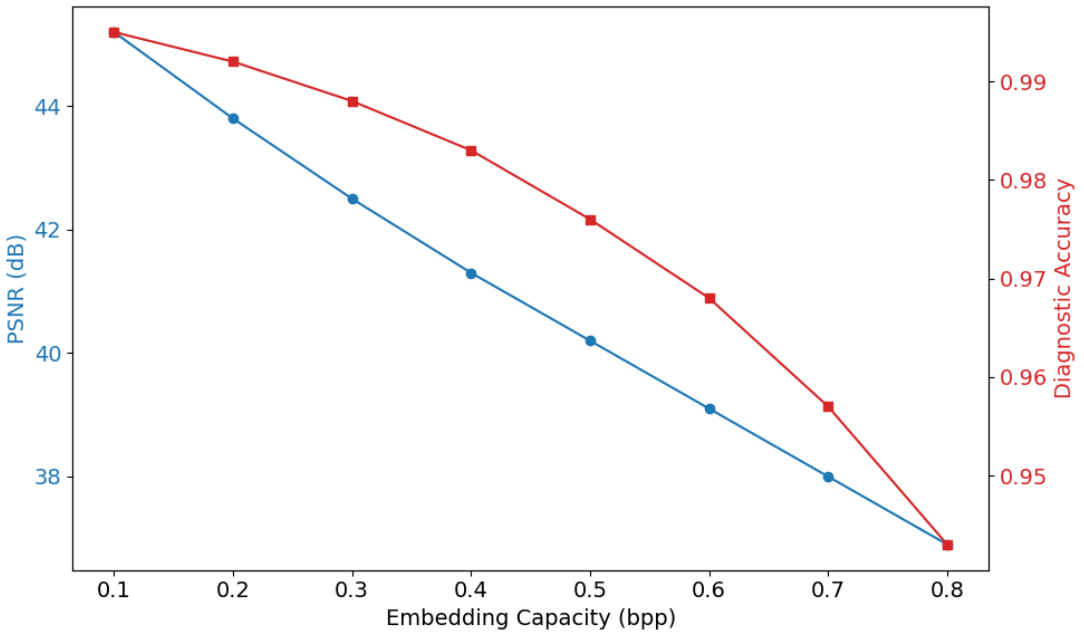

Fig. 12. Trade-off between Embedding Capacity, Image Quality, and Diagnostic Value.

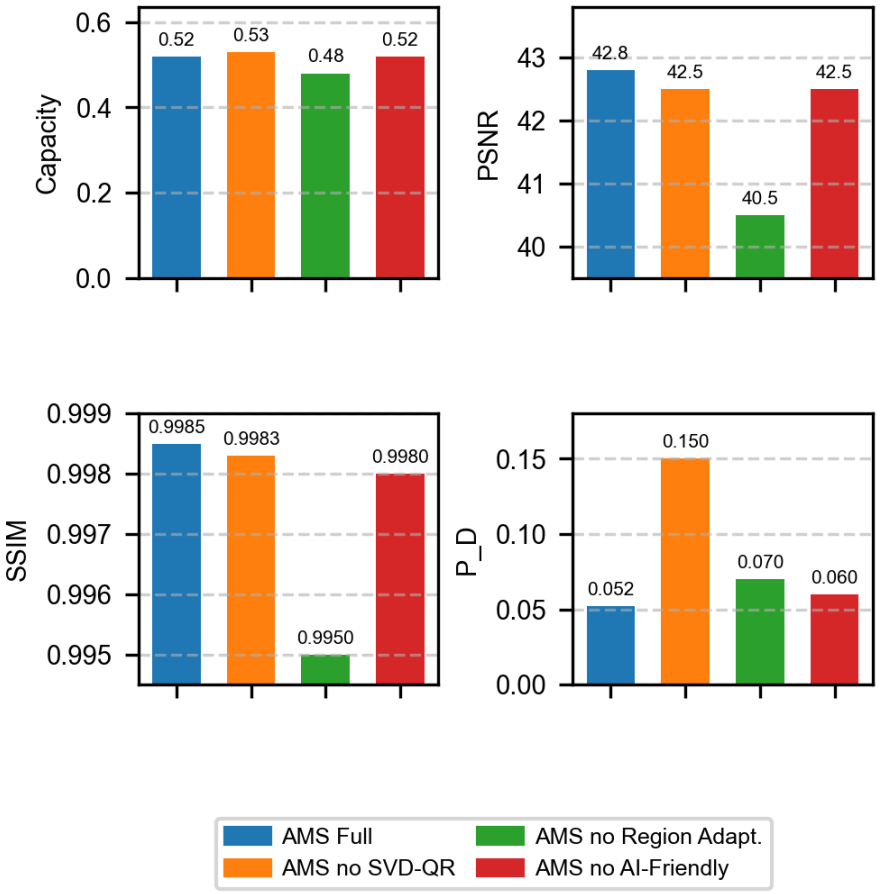

Fig. 13. Impact of Components on Performance Metrics.

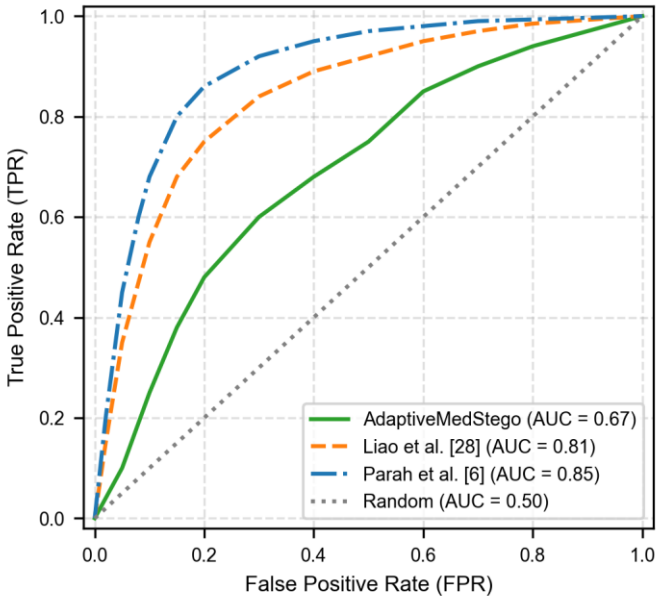

Fig. 14. ROC curves comparing the resilience of AdaptiveMedStego against Parah et al. [6] and Liao et al. [28] when subjected to deep learning-based steganalysis (Yedroudj-Net).

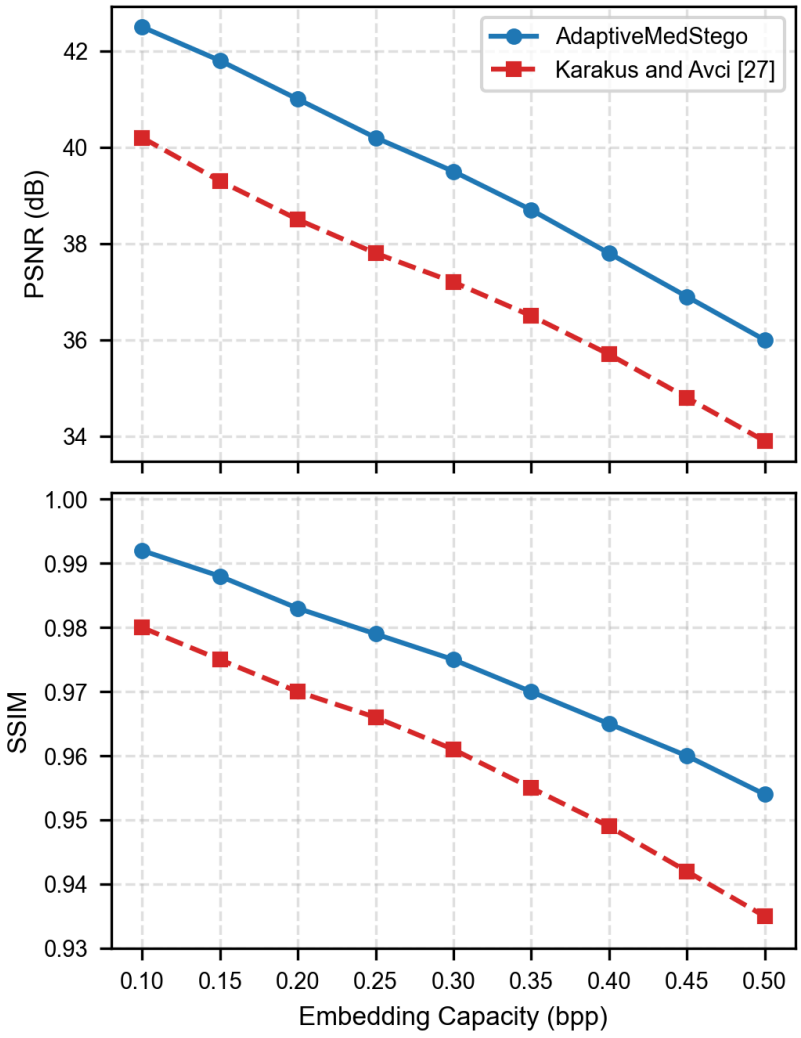

Fig. 15. Performance comparison on challenging ultrasound image dataset: (Top) PSNR vs. Embedding Capacity and (Bottom) SSIM vs. Embedding Capacity for AdaptiveMedStego and Karakus and Avci [27]. AdaptiveMedStego consistently maintains higher PSNR and SSIM values across various embedding rates, demonstrating its superior image quality preservation and adaptability to noisy US imagery.

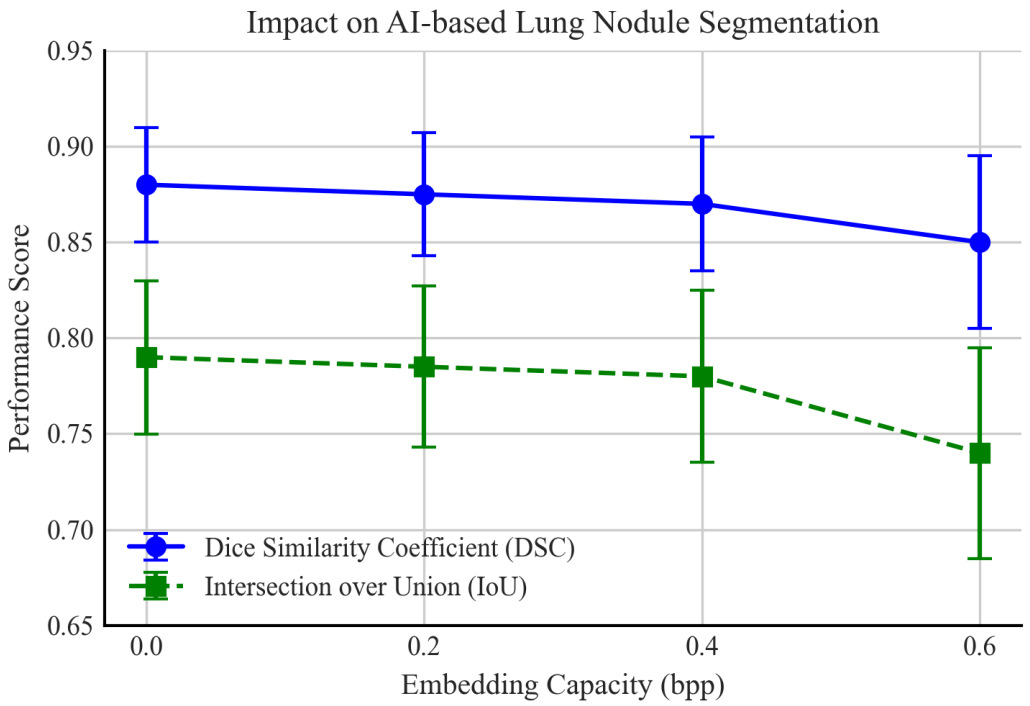

Fig. 16. Impact of AdaptiveMedStego on AI-based lung nodule segmentation. The Dice Similarity Coefficient (DSC) and Intersection over Union (IoU) of a pre-trained U-Net model show negligible decline when operating on stego-images with embedding capacities up to 0.4 bpp, and only a minor drop at 0.6 bpp. This demonstrates the effectiveness of the AI-friendly feature preservation mechanism in maintaining diagnostic integrity for automated systems.

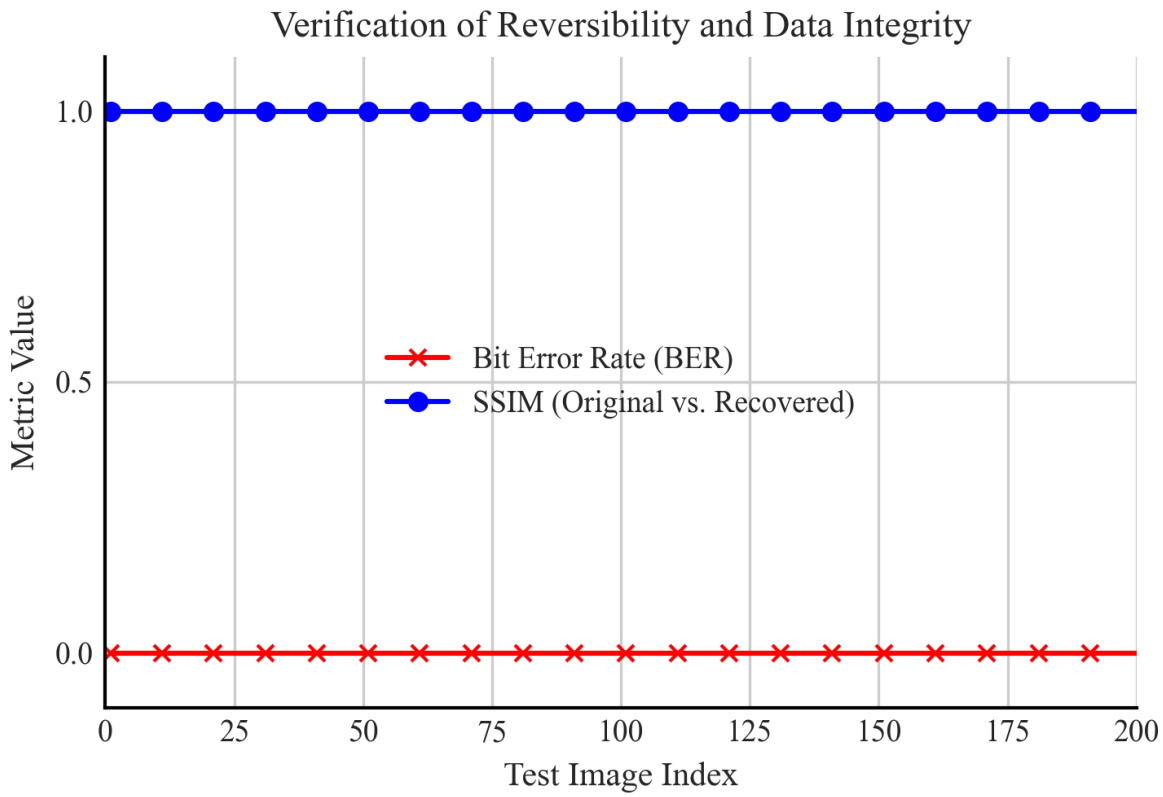

Fig. 17. Verification of reversibility and data integrity. The graph confirms that for all tested images, the Bit Error Rate (BER) of the extracted payload is zero, and the Structural Similarity Index (SSIM) between the original and recovered cover images is 1, indicating perfect, lossless reconstruction.

REFERENCES

[1] A. Kichloo, M. Albosta, K. Dettloff, F. Wani, Z. El-Amir, J. Singh, M. Aljadah, R. C. Chakinala, A. K. Kanugula, S. Solanki, and S. Chugh, "Telemedicine, the current COVID-19 pandemic and the future: a narrative review and perspectives moving forward in the USA", *Family Medicine and Community Health*, vol. 8, no. 3, e000530, 2020.

[2] D. He, S. Zeadally, and L. Wu, "Certificateless public auditing scheme for cloud-assisted wireless body area networks", *IEEE Systems Journal*, vol. 12, no. 1, pp. 64-73, 2015.

[3] S. A. Tovino, "The HIPAA Privacy Rule and the EU GDPR: Illustrative Comparisons", *Seton Hall Law Review*, vol. 47, no. 4, pp. 973-993, 2016.

[4] A. D. Dwivedi, G. Srivastava, S. Dhar, and R. Singh, "A decentralized privacy-preserving healthcare blockchain for IoT", *Sensors*, vol. 19, no. 2, article 326, 2019.

[5] Y. C. Hu, C. C. Lo, and W. L. Wu, "An Efficient Reversible Information Hiding Method for Medical Images", *Journal of Digital Imaging*, vol. 27, no. 6, pp. 721-731, 2014.

[6] S. A. Parah, F. Ahad, J. A. Sheikh, and G. M. Bhat, "Hiding clinical information in medical images: A new high capacity and reversible data hiding technique", *Journal of Biomedical Informatics*, vol. 108, article 103489, 2020.

[7] R. Thanki and K. Borisagar, "Hybrid SVD-DWT-based robust image steganography approach for e-healthcare applications", *Multimedia Tools and Applications*, vol. 82, no. 8, pp. 12089-12112, 2023.

[8] A. Al-Haj and D. Hussein, "DICOM-aware, reversible data hiding in medical images based on histogram shifting of difference values", *Signal Processing: Image Communication*, vol. 88, 115956, 2020.

[9] J. C. Dagadu and J. Li, "DWT-based adaptive steganography with QR code and LSB substitution for medical image security", *Security and Communication Networks*, 2021, article 6685801, 2021.

[10] Y. Liu, Q. Ai, Y. Wang, Y. Yu, B. Cui and Y. Xu, "An Improved LSML with Global and Local Label Correlation", *Engineering Letters*, vol. 33, no. 4, pp. 898-912, 2025.

[11] M. S. Subhedar and V. H. Mankar, "Current status and key issues in image steganography: A survey", *Computer Science Review*, vol. 13-14, pp. 95-113, 2014.

[12] A. F. Qasim, F. Meziane, and R. Aspin, "Digital watermarking: Applicability for developing trust in medical imaging workflows state of the art review", *Computer Science Review*, vol. 27, pp. 45-60, 2018.

[13] W. Pan, G. Coatrieux, N. Cuppens-Boulahia, F. Cuppens, and C. Roux, "Medical image integrity control combining digital signature and lossless watermarking", In *Data Privacy Management and Autonomous Spontaneous Security*, Springer, Berlin, Heidelberg, pp. 153-162, 2010.

[14] A. Al-Haj, "Providing integrity, authenticity, and confidentiality for header and pixel data of DICOM images", *Journal of Digital Imaging*, vol. 28, no. 2, pp. 179-187, 2015.

[15] I. Usman, A. Khan, A. Ali, and T. S. Choi, "Reversible steganography and authentication of medical images using improved LSB and discrete wavelet transform", *Journal of Medical Systems*, vol. 44, no. 2, pp. 1-14, 2020.

[16] A. A. Abd El-Latif, B. Abd-El-Atty, S. E. Venegas-Andraca, and W. Mazurczyk, "Efficient quantum-based security protocols for information sharing and data protection in 5G networks", *Future Generation Computer Systems*, vol. 100, pp. 893-906, 2019.

[17] Y. Liu, X. Qu, and G. Xin, "A ROI-based reversible data hiding scheme in encrypted medical images", *Journal of Visual Communication and Image Representation*, vol. 39, pp. 51-57, 2016.

[18] M. Jain, S. Rani, and A. Osuri, "Reversible data hiding in encrypted images using two-dimensional histogram modification", *Signal Processing: Image Communication*, vol. 82, article 115747, 2020.

[19] J. Uthayakumar, T. Vengattaraman, and P. Dhavachelvan, "A survey on data compression techniques: From the perspective of data quality, coding schemes, data type and applications", *Journal of King Saud University-Computer and Information Sciences*, vol. 31, no. 4, pp. 426-457, 2019.

[20] G. Rajini and R. Bhavani, "Automatic detection of speckle and Gaussian noise from ultrasound images using improved median filter and weighted mean filter", *Soft Computing*, vol. 24, no. 20, pp. 15441-15452, 2020.

[21] R. Singh and A. Khare, "Fusion of multimodal medical images using Daubechies complex wavelet transform–A multiresolution approach", *Information Fusion*, vol. 19, pp. 49-60, 2014.

[22] R. Nithya and B. Santhi, "Classification of normal and abnormal patterns in digital mammograms for diagnosis of breast cancer", *International Journal of Computer Assisted Radiology and Surgery*, vol. 13, no. 5, pp. 783-794, 2018.

[23] Y. Gan, Q. Zhao, Y. Lin, and M. Zhu, "Contrast enhancement for medical images based on image decomposition and fusion", *Multimedia Tools and Applications*, vol. 78, no. 3, pp. 3521-3540, 2019.

[24] F. Y. Shih and Y. T. Tseng, "Combined wavelet-based image enhancement and fuzzy ARTMAP for brain tumor detection", *International Journal of Imaging Systems and Technology*, vol. 15, no. 2, pp. 97-105, 2005.

[25] S. G. Armato III, G. McLennan, L. Bidaut, M. F. McNitt-Gray, C. R. Meyer, A. P. Reeves, and L. P. Clarke, "The Lung Image Database Consortium (LIDC) and Image Database Resource Initiative (IDRI): A completed reference database of lung nodules on CT scans", *Medical Physics*, vol. 38, no. 2, pp. 915-931, 2011.

[26] D. C. V. Essen, K. Ugurbil, E. Auerbach, D. Barch, T. E. J. Behrens, R. Bucholz, and E. Yacoub, "The Human Connectome Project: A data acquisition and analysis study", *NeuroImage*, vol. 62, no. 4, pp. 2222-2231, 2012.

[27] S. Karakus and E. Avci, "A new image steganography method with optimum pixel similarity for data hiding in medical images", *Medical hypotheses*, vol. 139, article 109691, 2020.

[28] X. Liao, J. Yin, M. Chen, Z. Qin, "Adaptive payload distribution in multiple images steganography based on image texture features", *IEEE Transactions on Dependable and Secure Computing*, vol. 19, no. 2, pp. 897-911, 2020.

[29] A. Sukumar, V. Subramaniyaswamy, L. Ravi, V. Vijayakumar, and V. Indragandhi, "Robust image steganography approach based on RIWT-Laplacian pyramid and histogram shifting using deep learning", *Multimedia Systems*, vol. 27, pp. 651-666, 2021.

[30] A. A. Abd El-Latif, B. Abd-El-Atty, S. E. Venegas-Andraca, H. Elwahsh, M. J. Piran, and A. K. Bashir, "Quantum-inspired blockchain-based cybersecurity: Securing smart edge utilities in 6G networks", *Information Processing & Management*, vol. 59, no. 2, article 102846, 2022.

[31] Yedroudj M., Comby F., Chaumont M. Yedroudj-Net: An efficient

CNN for spatial steganalysis. 2018 IEEE International Conference on Acoustics, Speech and Signal Processing (ICASSP), Calgary, Alberta, Canada, 2018: 15-20.

[32] Chen Y, Zhang C, Liu L, et al. USCL: pretraining deep ultrasound image diagnosis model through video contrastive representation learning. Medical Image Computing and Computer Assisted Intervention – MICCAI 2021: 24th International Conference, Strasbourg, France, 2021: 627-637.

Ya Qiu received the B.S. degree in computer application and technology from Henan Normal University, China, in 2005, the M.S. degree in computer application and technology from Xihua University, China, in 2010. She is currently a Lecturer and Head of the Department of Big Data Technology, School of Computer and Software, Nanyang Institute of Technology, China. Her current research directions are deep learning, computer vision and big data technology.

Xinchao Wang received the B.S. degree in Electronic Information Engineering from Xinyang Normal University, China, in 2007. He joined Nanyang Vocational College of Agriculture in 2013 and is currently a Lecturer. His research directions are electronic information engineering, electronic science and technology.

Chenrui Fu is currently working toward the bachelor's degree in software engineering with the School of Computer and Software, Nanyang Institute of Technology, Nanyang, China. His research interests include deep learning and object detection.

Xingyu Kang is currently working toward the bachelor's degree in software engineering with the School of Computer and Software, Nanyang Institute of Technology, Nanyang, China. His research interests include deep learning and image processing.

Yuhao Cui is currently working toward the bachelor's degree in software engineering with the School of Computer and Software, Nanyang Institute of Technology, Nanyang, China. His research interests include deep learning and image processing.